Asymptotic diffusion limit of cell temperature discretisation schemes for thermal radiation transport[☆]

Richard P. Smedley-Stevenson[a,b,*], Ryan G. McClarren[c,**]

[a] *AWE PLC, Aldermaston, Reading, Berkshire, RG7 4PR, UK*
[b] *Department of Earth Science and Engineering, Imperial College London, SW7 2AZ, UK*
[c] *Department of Nuclear Engineering, Texas A & M University, College Station, TX 77843-3133, USA*

Abstract

This paper attempts to unify the asymptotic diffusion limit analysis of thermal radiation transport schemes, for a linear discontinuous representation of the material temperature reconstructed from cell centred temperature unknowns, in a process known as 'source tilting'. The asymptotic limits of both Monte Carlo (continuous in space) and deterministic approaches (based on linear discontinuous finite elements) for solving the transport equation are investigated in slab geometry. The resulting discrete diffusion equations are found to have nonphysical terms that are proportional to any cell-edge discontinuity in the temperature representation. Based on this analysis it is possible to design accurate schemes for representing the material temperature, for coupling thermal radiation transport codes to a cell centred representation of internal energy favoured by ALE (arbitrary Lagrange-Eulerian) hydrodynamics schemes.

Keywords:
Source tilting, IMC, SIMC, linear discontinuous, asymptotic diffusion limit

[*] Principal corresponding author
[**] Corresponding author
Email addresses: richard.smedley-stevenson@awe.co.uk (Richard P. Smedley-Stevenson), rmcclarren@ne.tamu.edu (Ryan G. McClarren)

1. Introduction

High-energy density physics (HEDP) calculations to simulate experiments, such as inertial confinement fusion or high-mach number shock interactions, require the combination of two disparate fields of computational physics: hydrodynamics and thermal radiation transport. Computational hydrodynamics and radiation transport each have unique approaches to numerically solving the constituent partial differential equations. For example, radiation transport methods, in general, need discretizations designed to preserve the asymptotic diffusion limit of transport, often requiring several unknowns per spatial cell. On the other hand, hydrodynamics methods often use a single degree of freedom per spatial cell, which can lead to unexpected difficulties when coupling the two methods. This paper focuses on one particular aspect of this coupling: the coupling of hydrodynamics codes that use a cell centred treatment of the internal (material) energy to Monte Carlo and deterministic solutions of time dependent thermal radiation transport problems. In such an arrangement, the corresponding first-order accurate representation of the material temperature is insufficient to facilitate accurate computation of the thermal energy transport processes for algorithms which properly account for the directionality of the radiation field when the computational mesh does not resolve the radiation mean-free path.

Discrete diffusion schemes also need to make use of a higher order representation of the material temperature in order to avoid problems with excess numerical diffusion. However, this can be overcome by using a mixed element formulation which decomposes the second order diffusion equation into a set of coupled first order equations. A number of schemes exist which produce accurate solutions to this set of equations based on edge-based representations of the normal component of the flux vector [1, 2].

Deterministic transport algorithms based on discontinuous finite element formulations perform best if they use a nodal representation of the material temperature field, rather than the piecewise constant representation inherited from the hydrodynamics algorithm, which produces first order convergence with respect to the mesh spacing. In addition to recovering a second order convergence rate for sufficiently fine meshes, this paper demonstrates that a nodal treatment is essential in order to ensure accurate results in the asymptotic diffusion limit for both deterministic and Monte Carlo transport algorithms.

The asymptotic diffusion limit refers to meshes which are sufficiently fine

that they resolve the transport processes on the coarser length-scale associated with the diffusion of radiation energy through opaque media, but where it is impractical to resolve down to a photon mean free path. Schemes which do not perform well in this limit are generally unsuitable for modelling problems such as laser hohlraums, where the optical depth of the walls and the capsule are so large that it is impractical to use meshes with more than a few tens of cells through their respective thicknesses, especially for 3D simulations.

While our focus is on deterministic schemes based on the use of discontinuous finite elements for modelling the spatial variations, we acknowledge that it is possible to develop accurate schemes for solving the transport equation based on enforcing particle balance in local sub-volumes. The family of corner balance transport schemes splits a mesh of arbitrary polygonal elements into a set of sub-cells (corners) and couples the transport equation in each sub-volume to a set of independent piecewise constant material temperature values [3]. This approach is similar in spirit to the use of node centred temperatures, as there is still the requirement to model the variation of the material temperature within each sub-element in order to produce accurate results in the diffusion limit. Another way for deterministic transport algorithms to implement a nodal representation of the temperature in practice is to have the the radiation solver "own" a slope of the temperature in each cell that is not communicated to the hydrodynamics scheme[4]. This arrangement can lead to discontinuities in the temperature representation.

We analyse the asymptotic diffusion limit of both deterministic and Monte Carlo transport schemes in slab geometry, illustrating the close correspondence between the results. This leads us towards the formulation of discrete diffusion equations for the mesh cells which are approximations to the energy balance equation satisfied by Monte Carlo transport schemes and deterministic transport discretisations based on the use of linear discontinuous finite elements.

These discrete equations allow us to synthesize the results of the transport solutions on coarse meshes, as well as highlighting the most important aspects of the algorithm used to construct a higher order representation of material temperature suitable for use in the transport simulations. This theoretical underpinning is essential in order to guide the search for improved tilt schemes towards the most profitable avenues for future research.

Initially we consider the behaviour of a purely absorbing medium. This analysis is then extended to consider scattering problems, where the scatter-

ing is assumed to be a consequence of the semi-implicit temporal discretisation techniques which are commonly employed to overcome the time-step constraints due to the stiff coupling associated with the energy exchange term. These techniques are observed to improve the spatial convergence behaviour and this is confirmed by the asymptotic analysis. Unfortunately they also degrade the temporal accuracy of the results, leading to an interplay between the spatial and temporal resolution which can produce misleading results in convergence studies.

2. Problem description

We consider the solution of the coupled thermal radiation transport equation [5],

$$\frac{1}{c}\frac{\partial \Psi}{\partial t} + \mu \frac{\partial \Psi}{\partial x} + \sigma \Psi = \sigma \Phi \tag{1a}$$

and material energy equation,

$$(\rho C_V)\frac{\partial T}{\partial t} = 2\pi \int_{-1}^{1} \sigma(\Psi - \Phi) d\mu, \tag{1b}$$

for a purely absorbing slab in a grey medium. In these equations, x is the spatial variable, t time variable, μ is the cosine of the angle between a photon's direction-of-flight and the x-axis, $\Psi(\mu, x, t)$ is the intensity of thermal radiation, $\sigma(x, t)$ is the absorption opacity, c is the speed of light. The material temperature is denoted by $T(x, t)$, and $\rho C_V(x, t)$ is the heat capacity (the material density times the specific heat). The quantity $\Phi(x, t) \equiv \Phi(T(x, t))$ is the thermal emissivity, which is a Planckian blackbody emission source integrated over all frequency:

$$\Phi(T) = \frac{acT^4}{4\pi}, \tag{2}$$

where $a = 4\sigma_{\text{sb}}/c$ (σ_{sb} is the Stefan-Boltzmann constant).

In the asymptotic diffusion limit this reduces to a single equilibrium diffusion equation[6],

$$(\rho C_V)\frac{\partial T}{\partial t} + \frac{1}{c}\frac{\partial \Phi}{\partial t} = \nabla \cdot \left(\frac{1}{3\sigma}\nabla \Phi\right) \tag{3}$$

and our source tilt schemes should produce an accurate discretisation of this equation for meshes capable of resolving the spatial variation of Φ (in the

asymptotic diffusion limit where $\sigma\Delta x \gg 1$), rather than needing to resolve the radiation mean free path σ^{-1}.

We are interested in solving the coupled system of equations in the context of radiation-hydrodynamics when it is coupled to a set of hydrodynamic equations, such as the Euler equations, for the evolution of the material density, velocity, and internal energy. In this context, there is a separate discretization for the hydrodynamic system. In many cases, the internal energy, and therefore, the temperature are represented using a piecewise constant representation. For this reason, we will discretise the material energy equation in space using a piecewise constant representation. Despite the piecewise constant representation of the temperature, the thermal emissivity is allowed to have a piecewise linear variation (derived from the cell temperatures) for use in the transport/material system (1). As we will show, this is essential in order to prevent excess numerical diffusion in the transport equation. The aim of this paper is to derive a single equation for the energy flow in the equilibrium diffusion limit as a function of the piecewise linear emissivities.

The slab is subdivided into cells with piecewise constant material properties in each cell. We start by establishing our notation. The spatial domain extends from $x = 0$ to $x = L$ and is subdivided into N cells. The cells, which are not necessarily equally spaced, are given an index i extending from from 1 and to N, while the nodes are labelled with half indices starting with $x_{\frac{1}{2}} = 0$ and extending to $x_{N+\frac{1}{2}} = L$. We define the width of cell i, $\Delta x_i = x_{i+\frac{1}{2}} - x_{i-\frac{1}{2}}$, the cell absorption cross section σ_i (in units of inverse length), which is assumed to be independent of frequency, and from these the dimensionless optical depth $\tau_i = \sigma_i \Delta x_i$. We also define a set of cell centred heat capacities $(\rho C_V)_i$ so that the internal energy in cell i is given by $(\rho C_V)_i T_i$ per unit volume; for simplicity we assume that the heat capacities are constant i.e. the internal energy is a linear function of temperature.

The cell temperatures are assumed to have a piecewise constant variation. We can use them to define a corresponding set of nodal, i.e., cell-edge, T^4 values and from these the equilibrium radiation energy densities $U(T) = (4\pi/c)\Phi(T) = aT^4$. Using the piecewise constant temperatures to define a piecewise linear emissivity is commonly referred to 'source tilting' because the emissivity is allowed to have a linear variation within each element.

Φ is defined to have a linear discontinuous (LD) variation, i.e., the node values are defined locally in each cell i, with the left value $\Phi_{i,L}$ corresponding to the value at node $i - \frac{1}{2}$ and the right value $\Phi_{i,R}$ corresponding to the

value at node $i+\frac{1}{2}$. For a continuous reconstruction procedure we can define unique values at each node i.e. $\Phi_{i,R} = \Phi_{i+1,L} = \Phi_{i+\frac{1}{2}}$ at the interior mesh nodes. Internal to the element the temperature varies according to:

$$\Phi(x,t) = \Phi_{i,L}(t)b_1(x) + \Phi_{i,R}(t)b_2(x) \qquad x \in [x_{i-\frac{1}{2}}, x_{i+\frac{1}{2}}], \tag{4}$$

where,

$$b_1(x) = \frac{x_{i+\frac{1}{2}} - x}{\Delta x_i}, \qquad b_2(x)\frac{x - x_{i-\frac{1}{2}}}{\Delta x_i}.$$

The spatial variation of Φ is illustrated in figure 1.

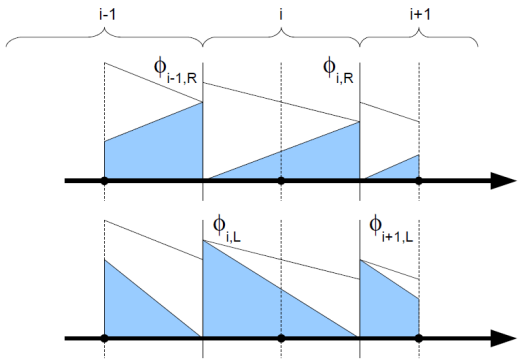

Figure 1: Plot of $\Phi(x,t)$ in terms of the discontinuous nodal values $\Phi_{i,L}(t)$ and $\Phi_{i,R}(t)$, illustrating how it can be decomposed into separate contributions from the right (top) and left (bottom) basis function in each cell i. The solid lines are the value of $\Phi(x,t)$ in each cell.

We note that in many numerical treatments, the underlying temperature could also be assumed to have a linear discontinuous spatial variation independent of the variation assumed for Φ, so these functions have consistent values only at the nodes of the element (i.e., a linear temperature is not the same as a linear emissivity). This potential inconsistency in the formulation has been investigated for deterministic calculations by Morel et al. [7] and for Monte Carlo by Smedley-Stevenson [8]. For the purposes of this asymptotic analysis it is sufficient to concentrate on modelling the evolution of the cell averaged temperatures.

The expression for the emissivity can be substituted into the right hand side of the photon transport equation, Eq. (1a):

$$\frac{1}{c}\frac{\partial \Psi}{\partial t} + \mu\frac{\partial \Psi}{\partial x} + \sigma_i\Psi = \sigma_i\Phi = \sigma_i\left(\Phi_{i,L}b_1(x) + \Phi_{i,R}b_2(x)\right) \tag{5}$$

where all quantities in this expression aside from the basis functions have an implied time-dependence which we have omitted. This is coupled to a cell-averaged version of the material equation, Eq. (1b):

$$(\rho C_V)_i \frac{\partial T_i}{\partial t} \Delta x_i = 2\pi \int_{x_{i-\frac{1}{2}}}^{x_{i+\frac{1}{2}}} \int_{-1}^{1} \sigma_i (\Psi(\mu, x) - \Phi(x)) d\mu dx \tag{6}$$

The boundaries of the problem are assumed to be freely radiating with an isotropic incident source $\Psi(\mu, x) = \Phi_L$ at $x_{\frac{1}{2}}$ for $\mu > 0$ and $\Psi(\mu, x) = \Phi_R$ at $x_{N+\frac{1}{2}}$ for $\mu < 0$, which is sufficient for the problems we are interested in studying. This avoids having to treat the issues associated with unresolved boundary layers induced by the directionality of the radiation field incident at the ends of the domain, which would act as a distraction to the conclusions of the analysis presented in this paper.

3. Spatially continuous transport equation

Our aim is to derive an analytic expression for the energy transport between neighbouring cells in terms of the node centred unknowns used to represent the spatial variation of the emissivity, for the spatially continuous transport equation corresponding to the use of a Monte Carlo method (or alternatively a mesh converged deterministic solution method) to solve the transport equation. By assuming the cells are optically thick, this problem reduces to that of calculating the energy flow across the cell interfaces, treating each pair of cells as two adjacent half-spaces with a linearly varying source in each region.

In the energy balance equation we assume that the radiation and material are in thermal equilibrium. This is not a significant assumption, as the optically thick cell assumption ensures that any boundary layers in the radiation field due to discontinuities in Φ are localised to the cell edges and do not significantly affect the mean value of the radiation energy density when averaged across the entire cell width. Furthermore, the contribution from this term is insignificant for most problems, as the energy density is dominated by the contribution from the material. A less accurate alternative approach would be to simply neglect this term in the energy equation.

Densmore has performed a comprehensive analysis of the asymptotic diffusion limit of the continuous transport problem for a linear discontinuous treatment of the source term [9]. Rather than repeating his analysis, we focus on generating approximate solutions of the Schwartzschild-Milne integral

equation appropriate for optically thick meshes, but relax the assumption of a spatially constant scattering ratio. Our aim is to produce a set of equations which enable predictions to be made about the diffusion limit behaviour for a given source tilt scheme.

3.1. Interface fluxes

We start off by deriving a cell energy balance equation for the equilibrium energy density. Integrating the transport equation over space and angle (and making use of the assumption that the radiation is in thermal equilibrium with the material,which is valid away from boundary layers, leads to:

$$\begin{aligned}\left[(\rho C_V)_i \frac{\partial T_i}{\partial t} + \frac{\partial U_i}{\partial t}\right] \Delta x_i &= -2\pi \int_{x_{i-\frac{1}{2}}}^{x_{i+\frac{1}{2}}} \int_{-1}^{1} \mu \frac{\partial}{\partial x} \Psi(x,\mu) d\mu dx \\ &= -2\pi \int_{-1}^{1} \mu (\Psi(x_{i+\frac{1}{2}},\mu) - \Psi(x_{i-\frac{1}{2}},\mu)) d\mu \\ &= F(x_{i+\frac{1}{2}}) - F(x_{i-\frac{1}{2}}),\end{aligned} \tag{7}$$

where

$$\begin{aligned}U_i \Delta x_i &= \frac{4\pi}{c} \int_{x_{i-\frac{1}{2}}}^{x_{i+\frac{1}{2}}} \Phi(x) dx \\ &= \frac{2\pi}{c} \left(\Phi_{i,L} + \Phi_{i,R}\right) \Delta x_i = \frac{4\pi}{c} \overline{\Phi}_i \Delta x_i\end{aligned} \tag{8}$$

and the radiation flux is $F(x)$. We are left with the problem of estimating the net radiation flux across the boundaries, $F(x_{i+\frac{1}{2}}) - F(x_{i-\frac{1}{2}})$, in order to determine the rate of energy transport.

3.2. Purely absorbing problems

In Monte Carlo methods for thermal radiative transfer, when the time scale of radiation emission and absorption is resolved by the time step, the coupled system of equations reduces to a transport equation for a pure absorber with a fixed source which can be solved independently from the material energy equation. In this section we investigate this case; later we will examine the case where the emission and absorption processes are not resolved and an effective scattering term is introduced.

To model the thermal emission term in the transport equation we source radiation isotropically according to this spatial emission profile and then

propagate it through the medium and deposit the energy in the appropriate cells to model the absorption term. The contributions to the emission can be split into the $2N$ individual contributions from the finite element basis functions, reducing this problem to one of modelling the propagation of the left and right element basis functions for a single reference element extending from $\hat{x} = 0$ to $\hat{x} = 1$. Furthermore, symmetry means that results for the right basis function can be derived directly from those for the left basis function by replacing $\hat{x}$ by $1 - \hat{x}$.

Ignoring time of flight effects (which are insignificant for optically thick problems) allows us drop the time derivative from the transport equation when evaluating the radiation flux, which leads to a balance equation for the total energy in each cell as a function of the nodal temperatures in this and the neighbouring cells in the absence of spatial discretisation errors in modelling the transport problem; this allows us to study the behaviour of the Monte Carlo method applied to this transport problem.

The corresponding balance equation is given by:

$$\begin{aligned}
&\frac{1}{4\pi}\left[(\rho C_V)_i \frac{\partial T_i}{\partial t} + \frac{\partial U_i}{\partial t}\right]\Delta x_i = \\
&-\sigma_i\left[\Phi_{i,L}L_{i,L\to i-1} + \Phi_{i,R}L_{i,R\to i-1}\right] + \sigma_{i+1}\left[\Phi_{i+1,L}L_{i+1,L\to i} + \Phi_{i+1,R}L_{i+1,R\to i}\right] \\
&-\sigma_i\left[\Phi_{i,L}L_{i,L\to i+1} + \Phi_{i,R}L_{i,R\to i+1}\right] + \sigma_{i-1}\left[\Phi_{i-1,L}L_{i-1,L\to i} + \Phi_{i-1,R}L_{i-1,R\to i}\right]
\end{aligned} \tag{9}$$

for interior cells $2 \leq i \leq N-1$, while for the boundary cells we have:

$$\begin{aligned}
\frac{1}{4\pi}\left[(\rho C_V)_1 \frac{\partial T_1}{\partial t} + \frac{\partial U_1}{\partial t}\right]\Delta x_1 \quad = \\
&-\sigma_1\left[\Phi_{1,L}L_{1,L\to 0} + \Phi_{1,R}L_{1,R\to 0}\right] \\
&+\sigma_2\left[\Phi_{2,L}L_{2,L\to 1} + \Phi_{2,R}L_{2,R\to 1}\right] \\
&-\sigma_1\left[\Phi_{1,L}L_{1,L\to 2} + \Phi_{1,R}L_{1,R\to 2}\right] \\
&+\tfrac{1}{4}\Phi_L
\end{aligned} \tag{10}$$

and

$$\begin{aligned}
\frac{1}{4\pi}\left[(\rho C_V)_N \frac{\partial T_N}{\partial t} + \frac{\partial U_N}{\partial t}\right]\Delta x_N \quad = \\
&-\sigma_N\left[\Phi_{N,L}L_{N,L\to N-1} + \Phi_{N,R}L_{N,R\to N-1}\right] \\
&+\tfrac{1}{4}\Phi_R \\
&-\sigma_N\left[\Phi_{N,L}L_{N,L\to N+1} + \Phi_{N,R}L_{N,R\to N+1}\right] \\
&+\sigma_{N-1}\left[\Phi_{N-1,L}L_{N-1,L\to N} + \Phi_{N-1,R}L_{N-1,R\to N}\right]
\end{aligned} \tag{11}$$

Here $L_{i,L\to i-1}$ represents the rate at which particles sourced according to the left basis function in cell i cross the left boundary and then deposit their energy in cell $i-1$, with the other quantities defined similarly. Here, we have precluded the possibility that particles can pass through cell $i-1$ into cell $i-2$ etc. Note that the factor 4π on the left hand side is a consequence of the definition of Φ and we could instead use $U=(4\pi/c)\Phi = aT^4$ on the right hand side of this expression so that this is expressed in terms of the radiation energy densities.

These terms can be evaluated explicitly according to the following formuli:

$$L_{i,L\to i-1} = L_{i,R\to i+1} = h_L(\tau_i)\Delta x_i \tag{12}$$

$$L_{i,L\to i+1} = L_{i,R\to i-1} = h_R(\tau_i)\Delta x_i \tag{13}$$

where

$$h_L(\tau) = \frac{1}{12\tau^2}\left((-2+3\tau)+(2-\tau+\tau^2)e^{-\tau}-\tau^3\mathrm{E}_1(\tau)\right) \tag{14}$$

$$h_R(\tau) = \frac{1}{6\tau^2}\left(1+(-1-\tau+\tau^2)e^{-\tau}-\tau^3\mathrm{E}_1(\tau)\right) \tag{15}$$

and $\mathrm{E}_1(x)=\int_x^\infty t^{-1}e^{-t}dt$ is the exponential integral. In the optically thick limit these expressions reduce to:

$$h_L(\tau) = \frac{1}{4\tau}-\frac{1}{6\tau^2} \tag{16}$$

$$h_R(\tau) = \frac{1}{6\tau^2} \tag{17}$$

The above expressions are derived directly from the formal solution of the steady-state transport equation i.e. the Schwarzschild-Milne equation for the radiation flux [10, Chapter 10].

To simplify the notation we introduce the following definitions for the jump across each interface $\delta\Phi_{i+\frac{1}{2}} = \Phi_{i+1,L}-\Phi_{i,R}$ and use the change within each cell to define a cell centred flux

$$F_i = -\frac{4\pi}{3\tau_i}(\Phi_{i,R}-\Phi_{i,L}) = -\frac{4\pi}{3\tau_i}\Delta\Phi_i \tag{18}$$

which is related to the slope of Φ within the element. Substituting the asymptotic values into the balance equation leads to:

$$\frac{1}{4\pi}\left[(\rho C_V)_i\frac{\partial T_i}{\partial t}+\frac{\partial U_i}{\partial t}\right]\Delta x_i = \\ +\tfrac{1}{4}\delta\Phi_{i+\frac{1}{2}}-\tfrac{1}{4}\delta\Phi_{i-\frac{1}{2}}-\tfrac{1}{8\pi}(F_{i+1}+F_i)+\tfrac{1}{8\pi}(F_{i-1}+F_i) \tag{19}$$

for $2 \leq i \leq N-1$, with similar expressions for the boundary cells. We do not explicitly cancel the contributions from the slopes within cell i, in order to aid the interpretation of these terms as a difference between the average values of the flux at the interfaces.

The jump terms in this expression do not depend on the material properties and therefore lead to unphysical energy exchange (e.g., even if $\sigma \to \infty$ there would still be energy flow across the cell boundary). The flux terms represent the energy change associated with discrete approximations to the equilibrium radiation fluxes on the faces of the element. Consequently, we must attempt to use a nearly continuous representation for the thermal emission term if we are to obtain accurate results from optically thick mesh Monte Carlo photon transport calculations.

3.2.1. Applicability to SIMC

By employing fully implicit time differencing with the discrete expression derived above, we should be able to predict the behaviour of the Symbolic Implicit Monte Carlo (SIMC) method [11] when combined with various source tilt strategies for determining the nodal values of Φ, for optically thick problems where it may not be possible to perform accurate Monte Carlo simulations. The slope can be calculated explicitly (a technique we refer to as a 'frozen tilt'), but with the emissivity scaled according to the fourth power of the cell averaged temperature such that the scheme remains stable.

We note that Clouët and Samba [12] obtained similar results in their asymptotic diffusion limit analysis of the SIMC method. Their work is more comprehensive, in that it extends to 2 and 3D geometries modelled with linear finite element basis functions, although they focused their attention on the asymptotic limit of the consistent linear discretisations rather than using their results to analyse source tilt schemes.

It is also useful in the context of this paper, as it provides additional information about the form of the multi-dimensional expressions, which are shown to be identical to those in slab geometry in 3-dimensions. The corresponding expressions for 2D problems contain additional corner terms (with a similar scaling to the flux terms), but these extra terms vanish for continuous tilt schemes. This provides additional confidence in the utility of the slab geometry studies for guiding the development of multi-dimensional tilt schemes.

3.3. Scattering problems

We now extend the above analysis to the case where some scattering is present in the system. This analysis is particularly applicable to the Implicit Monte Carlo (IMC) method. A new analytic solution of the two half-spaces problem has been derived [13], which generalised the coupling coefficients for the pure absorber problem to the case of different/non-zero scattering ratios in adjacent cells. Again we assume that the cells are sufficiently opaque that radiation cannot penetrate beyond the direct neighbours (and ignore time of flight effects) in order to derive the energy equation.

The corresponding transport problem is written as:

$$\mu\frac{\partial\Psi}{\partial x}+\sigma_i\Psi=(1-c_i)\sigma_i\left(\Phi_{i,L}b_1(x)+\Phi_{i,R}b_2(x)\right)+\frac{1}{2}c_i\sigma_i\int_{-1}^{1}\Psi\,d\mu \qquad (20)$$

where we have introduced a scattering term into the right hand side of the transport equation. This is the equation being solved in the grey Implicit Monte Carlo (IMC) method [14], where $f_i=1-c_i$ is the Fleck parameter (or Fleck factor) for cell i. f_i is a function of both the material properties and the time-step (Δt), which scales as $1/\Delta t$ in opaque strongly emitting cells to ensure that the scheme remains stable i.e. it prevents cells from emitting more energy than is stored locally in the material.

We note that the asymptotic scaling of the absorption and scattering terms is different depending on whether we are considering physical scattering or the scattering term results from the time discretisation. In this paper we focus on the latter case and investigate the case of a fixed Fleck parameter i.e. fixed $\sigma_i c\Delta t$ (fixed attenuation over the free streaming path length) for a purely absorbing problem, which means that the scattering ratio remains fixed as we investigate the limiting case of a large total cross-section (which corresponds to absorptions only)[6].

The transport equation can be transformed into optical depth co-ordinates in order to eliminate the effects of variable cross-sections, so that the coupling between cells is a function of the scattering ratios only. This allows us to derive equivalent expressions for the interface fluxes, which are valid provided that the cells remain optically thick i.e. provided $\sqrt{1-c_i}\sigma_i\Delta x_i\gg 1$.

The corresponding energy balance equation is given by:

$$\begin{aligned}\frac{1}{4\pi}\left[(\rho C_V)_i\frac{\partial T_i}{\partial t}+\frac{\partial U_i}{\partial t}\right]\Delta x_i = \\ +\eta(c_{i+1}\to c_i)(1-c_{i+1})\Phi_{i+1,L}-\eta(c_i\to c_{i+1})(1-c_i)\Phi_{i,R} \\ -\eta(c_i\to c_{i-1})(1-c_i)\Phi_{i,L}+\eta(c_{i-1}\to c_i)(1-c_{i-1})\Phi_{i-1,R} \\ -\tfrac{1}{4\pi}\theta(c_{i+1}\to c_i)F_{i+1}-\tfrac{1}{4\pi}\theta(c_i\to c_{i+1})F_i \\ +\tfrac{1}{4\pi}\theta(c_{i-1}\to c_i)F_{i-1}+\tfrac{1}{4\pi}\theta(c_i\to c_{i-1})F_i\end{aligned} \tag{21}$$

for $2\le i\le N-1$, with similar expressions at the boundaries.

Here the coefficient $\eta(c_1\to c_2)=\eta(c_2\to c_1)(1-c_2)/(1-c_1)$ is defined so that $4\pi\eta(c_1\to c_2)(1-c_1)\Phi$ is flux between two adjacent half spaces with scattering ratios c_1 and c_2, due to a spatially uniform isotropic source $(1-c_1)\Phi$ located in region 1; $\eta\to 1/4$ in purely absorbing regions. Likewise, the coefficient $\theta(c_1\to c_2)=1-\theta(c_2\to c_1)$ is defined so that $\theta(c_1\to c_2)F_1$ is the flux between two adjacent half spaces, for a linear (in space) isotropic emission profile $(1-c_1)\sigma_1\Phi(x)$ in region 1*; $\theta\to 1/2$ for regions with equal scattering ratios. The behaviour of these coefficients is described in greater detail in Appendix A.

Using these relationships, the equations simplify to:

$$\begin{aligned}\frac{1}{4\pi}\left[(\rho C_V)_i\frac{\partial T_i}{\partial t}+\frac{\partial U_i}{\partial t}\right]\Delta x_i = \\ +\eta(c_i\to c_{i+1})(1-c_i)\delta\Phi_{i+\frac{1}{2}}-\eta(c_i\to c_{i-1})(1-c_i)\delta\Phi_{i-\frac{1}{2}} \\ -\tfrac{1}{4\pi}((1-\theta(c_i\to c_{i+1}))F_{i+1}+\theta(c_i\to c_{i+1})F_i) \\ +\tfrac{1}{4\pi}((1-\theta(c_i\to c_{i-1}))F_{i-1}+\theta(c_i\to c_{i-1})F_i)\end{aligned} \tag{22}$$

for $2\le i\le N-1$ and at the boundaries we have:

$$\begin{aligned}\frac{1}{4\pi}\left[(\rho C_V)_1\frac{\partial T_1}{\partial t}+\frac{\partial U_1}{\partial t}\right]\Delta x_1 = \\ +\eta(c_2\to c_1)(1-c_2)\delta\Phi_{\frac{3}{2}}-\tfrac{1}{4}(1-\alpha(c_1))(\Phi_{1,L}-\Phi_L) \\ -\tfrac{1}{4\pi}((1-\theta(c_1\to c_2))F_2+\theta(c_1\to c_2)F_1) \\ +\tfrac{1}{4\pi}\theta(c_1\to 0)F_1\end{aligned} \tag{23}$$

*$\Phi(x)$ is the piecewise linear function whose slope is consistent with the value of $F_1=-(4\pi/3\sigma_1)\nabla\Phi(x)$ in region 1, which intercepts the axis at the interface between the two regions and is zero throughout region 2.

and:

$$\frac{1}{4\pi}\left[(\rho C_V)_N\frac{\partial T_N}{\partial t}+\frac{\partial U_N}{\partial t}\right]\Delta x_N = \\ +\tfrac{1}{4}(1-\alpha(c_N))(\Phi_R-\Phi_{N,R})-\eta(c_N\rightarrow c_{N-1})(1-c_N)\delta\Phi_{N-\frac{1}{2}} \quad (24)\\ -\tfrac{1}{4\pi}\theta(c_N\rightarrow 0)F_N \\ +\tfrac{1}{4\pi}((1-\theta(c_N\rightarrow c_{N-1}))F_{N-1}+\theta(c_N\rightarrow c_{N-1})F_N)$$

Here the boundary source terms are written in terms of the albedo for isotropic radiation incident on the respective surface i.e. $\alpha(c_1)=1-4\eta(0\rightarrow c_1)$ or $\alpha(c_N)=1-4\eta(0\rightarrow c_N)$ due to the presence of scattering.

From these expressions we see that the influence of the jump terms diminishes as the scattering ratio increases i.e., $\eta(c_1\rightarrow c_2)(1-c_1)$ decreases as $c_1\rightarrow 1$, and explains why the IMC method with large time-steps is less susceptible to the presence of discontinuities in the treatment of the thermal emission source term. Furthermore, we see that local differences in the scattering ratio (associated with the spatial variation of the Fleck parameter) lead to a bias in the flux across the interface towards the value in the cell with the larger scattering ratio.

Provided we have an efficient mechanism for evaluating these coupling coefficients for arbitrary values of the scattering ratios, then we could use the same strategy to simulate results from the IMC method as we propose for testing the results of the SIMC method. In this case, we treat the terms on the right hand side of the equation explicitly using the start of time-step values, taking advantage of the scaling of the jump terms which should ensure that the algorithm remains stable.

Finally, we restate the limitations of this analysis. It is constrained to meshes where the cell optical depth $\tau_i \gg 1/\sqrt{1-c_i}=1/\sqrt{f_i}\geq 1$. For a given mesh this places a lower limit on the Fleck parameter of 20–30$\times{\tau_i}^{-2}$, which prevents us from studying the behaviour as $f_i\rightarrow 0$. For smaller values of the Fleck parameter the assumption that the coupling is limited to nearest neighbours breaks down and we must solve the full transport problem in order to synthesize the IMC solution.

Densmore [9] followed this latter approach in order to show that the piecewise constant IMC scheme has a valid asymptotic diffusion limit provided that the Fleck parameter scales as ϵ^2. Furthermore, he has shown that the piecewise linear approach can produce accurate results for constant, ϵ and ϵ^2 scalings, for certain kinds of problem. Both the constant and ϵ scaling

results in his analysis are consistent with the results in this section, as they were derived by making the same assumption that the boundary layers associated with discontinuities in Φ are localised to the neighbouring cells i.e. $z_{i+1/2} \to \pm\infty$ for $x \in [x_i, x_{i+1}]$.

3.4. Asymptotic diffusion limit

In the asymptotic diffusion limit the constraint that coupling is limited to nearest neighbours translates to requiring $\sqrt{f} \gg \epsilon$, which can be satisfied for $f = f_0$ or $f = f_1\epsilon$. The property $\sqrt{f}\tau \gg 1$ in the discrete equations means that the coefficient in the unphysical jump terms will dominate that in the slope terms. Consequently, in order to obtain the correct asymptotic behaviour the magnitude of the jumps $\delta\Phi_{i+\frac{1}{2}}$ must be much smaller than the slopes $\Delta\Phi_i$.

For a piecewise constant treatment of Φ this can never be realized. However, depending on the details of the slope calculation, it may be possible to choose the mesh so that we can control the jumps in order to satisfy $\sqrt{f}\tau\delta\Phi \ll \Delta\Phi$; this is the argument made by Densmore. In this paper we make a stronger statement: by enforcing continuity we can guarantee that this relationship is satisfied, irrespective of the scaling of the Fleck parameter, for arbitrary meshes.

4. Spatially discretised transport equation

So far we have considered the behaviour of the spatially continuous transport equation. A set of discrete equations for the material temperature evolution have been derived as a function of the reconstructed emissivity values, assuming the cells are optically thick. It is useful to repeat the analysis for the spatially discretised transport equation in order to understand the convergence behaviour of deterministic transport methods based on the same source tilt methodologies.

We focus on linear discontinuous spatial discretisations of the transport equation, which are consistent with the linear treatment of the thermal emission term. In order to derive comparable expressions to those for the continuum transport equation we must perform an asymptotic diffusion limit analysis, scaling the terms in the transport equations so that we reveal the behaviour of the discrete equations as the mean free path becomes vanishingly small (for finite cell sizes), which is analogous to the nearest neighbour coupling assumption used previously.

To discretize the transport equation with linear discontinuous finite elements, we first write the spatial variation of Ψ inside element i as

$$\Psi(x,\mu,t) = \Psi_{i,L}(\mu,t)b_1(x) + \Psi_{i,R}(\mu,t)b_2(x) \qquad x \in [x_{i-\frac{1}{2}}, x_{i+\frac{1}{2}}] \tag{25}$$

In the subsequent derivation the μ and t dependence of these coefficients is omitted. If we substitute this form for Ψ into the transport equation and then multiply by $[b_1(x), b_2(x)]^t$ and integrate over cell i, we get

$$\frac{1}{c}\frac{\partial}{\partial t}\mathbf{M}_i\vec{\Psi}_i + \frac{\mu}{2}\begin{pmatrix}\Psi_{i,R} + \Psi_{i,L} - 2\Psi_{i-\frac{1}{2}} \\ -\Psi_{i,R} - \Psi_{i,L} + 2\Psi_{i+\frac{1}{2}}\end{pmatrix} + \sigma_{\mathrm{a},i}\mathbf{M}_i\vec{\Psi}_i \tag{26}$$

$$= \sigma_{\mathrm{a},i}\mathbf{M}_i\left[(1-c_i)\vec{\Phi}_i + \frac{c_i}{2}\int_{-1}^{1}\vec{\Psi}_i d\mu\right] \tag{27}$$

where $\vec{\Psi}_i = [\Psi_{i,L}, \Psi_{i,R}]^t$, $\vec{\Phi}_i = [\Phi_{i,L}, \Phi_{i,R}]^t$, and

$$\mathbf{M}_i = \frac{\Delta x_i}{6}\begin{pmatrix}2 & 1 \\ 1 & 2\end{pmatrix} \tag{28}$$

is the mass matrix for cell i. The values of Ψ at the boundary of the element, $\Psi_{i\pm\frac{1}{2}} = \Psi(x_{i\pm\frac{1}{2}}, \mu, t)$ are determined based on the value of μ:

$$\Psi_{i+\frac{1}{2}} = \begin{cases}\Psi_{i-1,R} & \mu > 0 \\ \Psi_{i,L} & \mu < 0\end{cases}$$

These values are chosen using the principle of upwinding: when μ is positive information flows from the left to the right, and therefore we interpret the value of Ψ at the interface as the value just to the left of the interface, $\Psi_{i-1,R}$.

Similarly, if we substitute the linear discontinuous forms of Ψ and Φ into the material energy equation, Eq. (1b), we get

$$(\rho C_{\mathrm{V}})_i\frac{\partial T_i}{\partial t} = 2\pi\int_{-1}^{1}(1-c_i)\sigma_{\mathrm{a},i}\left(\overline{\Psi}_i - \overline{\Phi}_i\right)d\mu \tag{29}$$

here $\overline{\Psi}_i = \frac{1}{2}(\Psi_{i,L} + \Psi_{i,R})$, and $\overline{\Phi}_i = \frac{1}{2}(\Phi_{i,L} + \Phi_{i,R})$. One characteristic of the linear discontinuous finite element method is that we can derive a cell

balance equation if we sum the rows of Eq. (26). Integrating the resulting equation over particle direction we get

$$(\rho C_{\mathrm{V}})_i \frac{\partial T_i}{\partial t} + \frac{\partial U_i}{\partial t} + \frac{F_{i+\frac{1}{2}} - F_{i-\frac{1}{2}}}{\Delta x_i} = 0, \tag{30}$$

where

$$F_{i+\frac{1}{2}} = 2\pi \left[\int_{-1}^{0} \mu \Psi_{i+1,L} \, d\mu + \int_{0}^{1} \mu \Psi_{i,R} \, d\mu \right] \tag{31}$$

and this has the same form as Eq. (7).

4.1. Asymptotic diffusion limit

To investigate the asymptotic diffusion limit of this system we apply the appropriate asymptotic scaling [15] to Eqs. (26) and (29)

$$\frac{\epsilon}{c}\frac{\partial}{\partial t_1}\mathbf{M}_i\vec{\Psi}_i + \frac{\epsilon^2}{c}\frac{\partial}{\partial t_2}\mathbf{M}_i\vec{\Psi}_i + \frac{\epsilon\mu}{2}\begin{pmatrix} \Psi_{i,R} + \Psi_{i,L} - 2\Psi_{i-\frac{1}{2}} \\ -\Psi_{i,R} - \Psi_{i,L} + 2\Psi_{i+\frac{1}{2}} \end{pmatrix} + \sigma_{\mathrm{a},i}\mathbf{M}_i\vec{\Psi}_i \tag{32a}$$

$$= \sigma_{\mathrm{a},i}\mathbf{M}_i \left[(1-c_i)\vec{\Phi}_i + \frac{c_i}{2}\int_{-1}^{1} \vec{\Psi}_i d\mu \right]$$

$$\epsilon(\rho C_{\mathrm{V}})_i \frac{\partial T_i}{\partial t_1} + \epsilon^2(\rho C_{\mathrm{V}})_i \frac{\partial T_i}{\partial t_2} = 2\pi \int_{-1}^{1} (1-c_i)\sigma_{\mathrm{a},i} \left(\overline{\Psi}_i - \overline{\Phi}_i \right) d\mu \tag{32b}$$

where the ϵ is the small (positive) asymptotic scaling parameter and we have introduced two time variables t_1 and t_2 corresponding to the fast time evolution which we associate with the presence of spurious large jump discontinuities in the source tilt and a slow time-scale corresponding to the physical evolution of the material temperature. We then expand Ψ in a power series of the form

$$(\cdot) = \sum_{l=0}^{\infty} \epsilon^l (\cdot)^{(l)} \tag{33}$$

and equate like orders of ϵ.

We do not expand either Φ or T in terms of a power series, but instead treat them both as $O(1)$ quantities, as the aim is to focus on the properties of the transport solution for a given source tilt prescription and study

the associated temperature evolution. Cancellations between terms in the resulting expressions will determine the precise order of their contributions to the cell energy balance expressions. $f = 1 - c$ is assumed to be an $O(1)$ quantity which depends on the ratio of time-step used in the simulation to the equilibration time of the medium; it is possible to repeat this analysis for other cases such as $f = O(\epsilon)$ or $f = O(\epsilon^2)$.

The $O(1)$ equations give

$$\Psi^{(0)}_{i,L} = \Phi_{i,L}, \quad \Psi^{(0)}_{i,R} = \Phi_{i,R} \tag{34a}$$

and

$$\overline{\Psi}^{(0)}_i = \overline{\Phi}_i \tag{34b}$$

which are completely consistent. Continuing the expansion to $O(\epsilon)$, the semi-discrete transport equation, Eq. (32a), can be written as

$$\vec{\Psi}^{(1)}_i = \frac{c_i}{2} \int_{-1}^{1} \vec{\Psi}^{(1)}_i d\mu - \frac{\mu}{\sigma_{\mathrm{a},i}} \mathbf{M}_i^{-1} \begin{pmatrix} \overline{\Phi}_i - \Psi^{(0)}_{i-\frac{1}{2}} \\ \Psi^{(0)}_{i+\frac{1}{2}} - \overline{\Phi}_i \end{pmatrix} \tag{35}$$

where we have multiplied this equation by $\sigma^{-1}_{\mathrm{a},i} \mathbf{M}_i^{-1}$ and

$$\Psi^{(0)}_{i+\frac{1}{2}} = \begin{cases} \Phi_{i-1,R} & \mu > 0 \\ \Phi_{i,L} & \mu < 0 \end{cases}$$

For non-zero scattering ratios we have an additional isotropic contribution to the first order intensity which can be evaluated by integrating this expression over angle and using the upwind values in the boundary terms.

$$\begin{aligned} \frac{c_i}{2} \int_{-1}^{1} \vec{\Psi}^{(1)}_i d\mu &= \frac{c_i}{(1-c_i)} \frac{1}{4\sigma_{\mathrm{a},i}} \mathbf{M}_i^{-1} \begin{pmatrix} -\delta\Phi_{i-\frac{1}{2}} \\ \delta\Phi_{i+\frac{1}{2}} \end{pmatrix} \\ &= \frac{c_i}{(1-c_i)} \frac{1}{2\sigma_{\mathrm{a},i}\Delta x_i} \begin{pmatrix} 2 & -1 \\ -1 & 2 \end{pmatrix} \begin{pmatrix} -\delta\Phi_{i-\frac{1}{2}} \\ \delta\Phi_{i+\frac{1}{2}} \end{pmatrix} \end{aligned} \tag{36}$$

which vanishes for continuous reconstructions. This can then be substituted

in the following expressions for the first order intensity

$$\Psi_{i,L}^{(1)} = \frac{c_i}{2} \int_{-1}^{1} \Psi_{i,L}^{(1)} d\mu + \frac{\mu}{\sigma_{\mathrm{a},i} \Delta x_i} \left(4\Phi_{i-\frac{1}{2}} + 2\Phi_{i+\frac{1}{2}} - 6\overline{\Phi}_i \right) \tag{37a}$$

$$\Psi_{i,R}^{(1)} = \frac{c_i}{2} \int_{-1}^{1} \Psi_{i,R}^{(1)} d\mu + \frac{\mu}{\sigma_{\mathrm{a},i} \Delta x_i} \left(-2\Phi_{i-\frac{1}{2}} - 4\Phi_{i+\frac{1}{2}} + 6\overline{\Phi}_i \right) \tag{37b}$$

The corresponding material energy equation (retaining terms up to $O(\epsilon^2)$) is given by

$$\epsilon (\rho C_{\mathrm{V}})_i \frac{\partial T_i}{\partial t_1} + \epsilon^2 (\rho C_{\mathrm{V}})_i \frac{\partial T_i}{\partial t_2} = 2\pi\epsilon \int_{-1}^{1} (1 - c_i) \sigma_{\mathrm{a},i} \left(\overline{\Psi}_i^{(1)} + \epsilon \overline{\Psi}_i^{(2)} \right) d\mu \tag{38}$$

which can be split into two equations corresponding to the two time-scales introduced earlier

$$(\rho C_{\mathrm{V}})_i \frac{\partial T_i}{\partial t_1} = 2\pi \int_{-1}^{1} (1 - c_i) \sigma_{\mathrm{a},i} \overline{\Psi}_i^{(1)} d\mu \tag{39}$$

$$(\rho C_{\mathrm{V}})_i \frac{\partial T_i}{\partial t_2} = 2\pi \int_{-1}^{1} (1 - c_i) \sigma_{\mathrm{a},i} \overline{\Psi}_i^{(2)} d\mu \tag{40}$$

To eliminate the first equation we require the right-hand side to vanish, which implies that the angular integral of the first order intensity integrates to zero over the cell. Using the upwind definition of the boundary values leads to the following solvability condition

$$\delta\Phi_{i+\frac{1}{2}} - \delta\Phi_{i-\frac{1}{2}} = O(\epsilon), \tag{41}$$

The $O(1)$ difference between the jump terms must vanish in the source tilt scheme in order to eliminate the contribution from the fast time variable t_1. This ensures that the energy transport associated with discontinuities in the reconstruction is of the same order as that due to the linearly anisotropic component of the radiation field, a prerequisite for a valid asymptotic diffusion limit. Reconstructions which fail to satisfy (41) have a spurious temperature evolution on the fast time-scale t_1, which artificially enhances the propagation of thermal waves in optically thick cells.

The solvability condition is automatically satisfied by continuous reconstructions (as the left-hand side is zero), or discontinuous reconstructions such as the frozen tilt scheme (discussed in section 3.2.1) where the discontinuities are constrained to be $O(\epsilon)$. Another possibility is that the mesh size scales with ϵ, but we already know that a piecewise constant treatment of the material temperature provides sufficient accuracy in this intermediate regime so long as the mesh resolution is sufficient to ensure that the cell optical depths are much less than one.

We now continue the analysis up to $O(\epsilon^2)$ in order to study the evolution on the slow time-scale, leading to the following expressions for the radiation field

$$\Psi_{i,L} = \Phi_{i,L} + \epsilon \left[\frac{c_i}{2} \int_{-1}^{1} \Psi_{i,L}^{(1)} d\mu + \frac{\mu}{\tau_i} \left(4\Phi_{i-\frac{1}{2}} + 2\Phi_{i+\frac{1}{2}} - 6\overline{\Phi}_i \right) \right] \tag{42a}$$

$$\Psi_{i,R} = \Phi_{i,R} + \epsilon \left[\frac{c_i}{2} \int_{-1}^{1} \Psi_{i,R}^{(1)} d\mu + \frac{\mu}{\tau_i} \left(-2\Phi_{i-\frac{1}{2}} - 4\Phi_{i+\frac{1}{2}} + 6\overline{\Phi}_i \right) \right] \tag{42b}$$

Using these equations we can compute the flux crossing the interface $i + \frac{1}{2}$ (between cells i and $i+1$)

$$\begin{aligned} \frac{F_{i+\frac{1}{2}}}{4\pi} = -\frac{1}{4}\delta\Phi_{i+\frac{1}{2}} &- \frac{\epsilon}{4} \left[\frac{c_{i+1}}{2} \int_{-1}^{1} \Psi_{i+1,L}^{(1)} d\mu - \frac{c_i}{2} \int_{-1}^{1} \Psi_{i,R}^{(1)} d\mu \right] \\ &- \epsilon \frac{1}{6\tau_i} \left(\Phi_{i,R} - 3\Phi_{i,L} + 2\Phi_{i-1,R} \right) \\ &- \epsilon \frac{1}{6\tau_{i+1}} \left(-2\Phi_{i+2,L} + 3\Phi_{i+1,R} - \Phi_{i+1,L} \right) + O(\epsilon^2) \end{aligned} \tag{43}$$

which can be written in the following simplified form

$$\begin{aligned} \frac{F_{i+\frac{1}{2}}}{4\pi} = -\frac{1}{4}(\Phi_{i+1,L}^{*} - \Phi_{i,R}^{*}) &\\ &- \epsilon \frac{1}{6\tau_i} \left(\Phi_{i,R} - 3\Phi_{i,L} + 2\Phi_{i-1,R} \right) \\ &- \epsilon \frac{1}{6\tau_{i+1}} \left(-2\Phi_{i+2,L} + 3\Phi_{i+1,R} - \Phi_{i+1,L} \right) + O(\epsilon^2) \end{aligned} \tag{44}$$

where

$$\begin{aligned}\vec{\Phi}_i^* &= \vec{\Phi}_i + \epsilon\frac{c_i}{2}\int_{-1}^{1}\vec{\Psi}_i^{(1)}d\mu \\ &= \vec{\Phi}_i + \frac{\epsilon}{2\tau_i}\frac{c_i}{(1-c_i)}\begin{pmatrix}2 & -1\\ -1 & 2\end{pmatrix}\begin{pmatrix}-\delta\Phi_{i-\frac{1}{2}}\\ \delta\Phi_{i+\frac{1}{2}}\end{pmatrix} \qquad (45)\end{aligned}$$

Using this relation in the scaled version of Eq. (30) gives

$$\begin{aligned}\frac{1}{4\pi}\left[\left((\rho C_{\mathrm{V}})_i\frac{\partial T_i}{\partial t_1}+\frac{\partial U_i^*}{\partial t_1}\right)+\epsilon\left((\rho C_{\mathrm{V}})_i\frac{\partial T_i}{\partial t_2}+\frac{\partial U_i^*}{\partial t_2}\right)\right]\Delta x_i \\ = +\frac{1}{4}(\Phi^*_{i+1,L}-\Phi^*_{i,R})-\frac{1}{4}(\Phi^*_{i,L}-\Phi^*_{i-1,R}) \\ +\epsilon\frac{1}{6\tau_{i+1}}\left(-2\Phi_{i+2,L}+3\Phi_{i+1,R}-\Phi_{i+1,L}\right) \\ +\epsilon\frac{1}{6\tau_i}\left(2\Phi_{i-1,R}+\Phi_{i,R}-3\Phi_{i,L}\right) \\ -\epsilon\frac{1}{6\tau_{i-1}}\left(\Phi_{i-1,R}-3\Phi_{i-1,L}+2\Phi_{i-2,R}\right) \\ -\epsilon\frac{1}{6\tau_i}\left(-2\Phi_{i+1,L}+3\Phi_{i,R}-\Phi_{i,L}\right)+O(\epsilon^2) \qquad (46)\end{aligned}$$

This equation is the deterministic analogue of the energy equation associated with the spatially continuous transport equation, for a linear discontinuous spatial discretisation. Here we have not discretised the angular variable, but we expect similar results to hold for any angular discretisation applied to the first order transport equation which allows us to upwind the boundary fluxes and is able to accurately resolve independent linear variations in angle over each half-space[†].

For the P_n method (with odd n) we can decompose the solution into left and right moving waves, prior to imposing the boundary conditions between elements[‡] and this technique has been used by one of the authors (McClarren) to solve the P_n equations [16, 17]. A similar technique is used in the

[†]Full range expansion techniques have this property, but converge more slowly than the equivalent half range expansions.

[‡]This demonstrates the well known equivalence between the P_{n-1} method and an S_n scheme with the corresponding Gauss-Legendre quadrature set.

RADIANT code developed at Imperial College [18] in collaboration with the other author (Smedley-Stevenson), which formulates the angularly discretised transport equation in terms of the characteristic variables associated with a particular angular discretisation and allows the same coding to be used for both S_n, P_n and wavelet discretisations of the angular variable.

4.1.1. Mass lumping

A similar (but more localised) expression can be derived if we apply mass lumping to the exchange terms

$$\frac{1}{4\pi}\left[\left((\rho C_{\mathrm{V}})_i\frac{\partial T_i}{\partial t_1}+\frac{\partial U_i^{*L}}{\partial t_1}\right)+\epsilon\left((\rho C_{\mathrm{V}})_i\frac{\partial T_i}{\partial t_2}+\frac{\partial U_i^{*L}}{\partial t_2}\right)\right]\Delta x_i$$
$$=+\frac{1}{4}(\Phi^{*L}_{i+1,L}-\Phi^{*L}_{i,R})-\frac{1}{4}(\Phi^{*L}_{i,L}-\Phi^{*L}_{i-1,R})$$
$$-\frac{\epsilon}{8\pi}(F_{i+1}+F_i)+\frac{\epsilon}{8\pi}(F_{i-1}+F_i)+O(\epsilon^2) \quad (47)$$

This is identical to the unlumped results for continuous reconstructions[§], but there are subtle differences in the behaviour for discontinuous reconstructions due to both the jump and flux terms. The definition of Φ^{*L} is consistent with the application of mass lumping to Eq. (45)

$$\vec{\Phi}_i^{*L} \;=\; \vec{\Phi}_i+\frac{\epsilon}{2\tau_i}\frac{c_i}{(1-c_i)}\begin{pmatrix}-\delta\Phi_{i-\frac{1}{2}}\\ \delta\Phi_{i+\frac{1}{2}}\end{pmatrix} \quad (48)$$

In the absence of scattering, if the spatial mesh for the unlumped transport equations is refined by subdividing the cells (and duplicating the material properties/interpolating the source term), the non-local coupling terms disappear and the asymptotic behaviour matches the lumped expressions on the original transport mesh. Mass lumping of the purely absorbing transport problem can therefore be interpreted as being equivalent to an arbitrary increase in the spatial resolution of the transport solution, for a fixed temperature grid i.e. it is identical to that of the continuum problem (see Eq. (19)).

4.2. Implications

We now pursue the implications of the asymptotic analysis. Firstly, we see that (as with the continuum transport problem) a continuous reconstruction

[§]Except at the problem boundaries, if the continuity is restricted to the problem interior.

will lead to the correct asymptotic behaviour corresponding to a particular discretisation of the diffusion equation, which is unaffected by mass lumping (except possibly at the problem boundaries).

4.2.1. Piecewise constant scheme

For a piecewise constant representation of Φ the solvability constraint for the $O(\epsilon)$ equations implies the following relationship between the cell temperatures

$$\Phi_{i+1} - 2\Phi_i + \Phi_{i-1} = O(\epsilon) \tag{49}$$

The steady-state solution will satisfy this equation (with zero on the right-hand side) i.e. Φ evolves towards a linear function of the mesh cell index, which matches the left and right boundary values. This is the correct steady-state solution for a constant opacity medium modelled with a uniform mesh, but represents a spurious discretisation of the equilibrium problem for non-uniform meshes/spatially varying opacities. For time dependent problems this scheme does not have a valid diffusion limit, irrespective of the details of the problem definition.

4.2.2. Discontinuous reconstructions

For general discontinuous reconstructions (which includes the piecewise constant representation as a special case) we have

$$\delta\Phi_{i+\frac{1}{2}} - \delta\Phi_{i-\frac{1}{2}} = O(1) \tag{50}$$

which implies an incorrect $O(\epsilon^{-1})$ scaling of the time derivative terms i.e. it results in the introduction of variations with respect to the spurious fast time-scale t_1. The total energy equation can now be written as

$$\begin{aligned}\frac{1}{4\pi}\left[\left((\rho C_{\mathrm{V}})_i\frac{\partial T_i}{\partial t_1} + \frac{\partial U_i^*}{\partial t_1}\right) + \epsilon\left((\rho C_{\mathrm{V}})_i\frac{\partial T_i}{\partial t_2} + \frac{\partial U_i^*}{\partial t_2}\right)\right]\Delta x_i \\ = +\frac{1}{4}(\Phi^*_{i+1,L} - \Phi^*_{i,R}) - \frac{1}{4}(\Phi^*_{i,L} - \Phi^*_{i-1,R}) + O(\epsilon)\end{aligned} \tag{51}$$

where the energy flow rate does not depend on either the mesh spacing or the optical properties of the medium. This is the discrete equation satisfied by reconstructions with unconstrained discontinuities, such as the traditional gradient based source tilt schemes. We can include the $O(\epsilon)$ term (with or without lumping) in order to increase the accuracy of the predicted asymptotic behaviour, noting that this term vanishes for the lumped treatment of piecewise constant temperatures.

5. Summary of the asymptotic analysis

In the preceding sections we have derived the corresponding total energy equation for both SIMC and IMC based Monte Carlo transport schemes which can be written in the following general form:

$$\begin{aligned}\frac{1}{4\pi}\left[(\rho C_V)_i\frac{\partial T_i}{\partial t}+\frac{\partial U_i}{\partial t}\right]\Delta x_i = \\ +\eta(c_i\rightarrow c_{i+1})(1-c_i)\delta\Phi_{i+\frac{1}{2}} \\ -\eta(c_i\rightarrow c_{i-1})(1-c_i)\delta\Phi_{i-\frac{1}{2}} \\ -\frac{1}{4\pi}((1-\theta(c_i\rightarrow c_{i+1}))F_{i+1}+\theta(c_i\rightarrow c_{i+1})F_i) \\ +\frac{1}{4\pi}((1-\theta(c_i\rightarrow c_{i-1}))F_{i-1}+\theta(c_i\rightarrow c_{i-1})F_i)\end{aligned} \tag{52}$$

and also for a linear discontinuous spatial discretisation:

$$\begin{aligned}\frac{1}{4\pi}\left[(\rho C_{\mathrm{V}})_i\frac{\partial T_i}{\partial t}+\frac{\partial U_i^*}{\partial t}\right]\Delta x_i = +\frac{1}{4}(\Phi^*_{i+1,L}-\Phi^*_{i,R})-\frac{1}{4}(\Phi^*_{i,L}-\Phi^*_{i-1,R}) \\ +\frac{1}{6\tau_{i+1}}\left(-2\Phi_{i+2,L}+3\Phi_{i+1,R}-\Phi_{i+1,L}\right) \\ +\frac{1}{6\tau_i}\left(2\Phi_{i-1,R}+\Phi_{i,R}-3\Phi_{i,L}\right) \\ -\frac{1}{6\tau_{i-1}}\left(\Phi_{i-1,R}-3\Phi_{i-1,L}+2\Phi_{i-2,R}\right) \\ -\frac{1}{6\tau_i}\left(-2\Phi_{i+1,L}+3\Phi_{i,R}-\Phi_{i,L}\right)\end{aligned} \tag{53}$$

which is the same except for the flux terms which now depend on the values of the emission profile in cells $i-2$ and $i+2$ as well as in the direct neighbours; we note that the lumped equations agree with the continuum transport results for the no scattering problem. These equations predict the energy flow rate for a given emission profile, showing how the source tilt scheme influences the energy balance in the problem, for problems modelled with optically thick cells.

We note that $U_i^* \rightarrow (4\pi/c)\overline{\Phi}_i$ which is the value determined from the source tilt rather than the value consistent with the cell centred temperature. Consequently, the source tilt may also affect the partitioning of energy

between the material and the radiation field as well as the energy flow rate. This value will generally be larger than the cell centred value derived from $(T_i)^4$. For a linear reconstruction the additional variations introduced by the tilt scheme bias the function so that it has a mean value up to 8 times larger in the most extreme case, for schemes which preserve the cell average temperature.

We note that similar results apply to schemes which subdivide the original cells into sub-elements with a reconstruction which maintains continuity within the element. These schemes have the benefit of reducing the size of the stencil in the asymptotic limit equations, thereby avoiding problems associated with the decoupling of the even and odd numbered cells in the problem interior which can lead to oscillatory solutions.

5.1. Discussion

It is immediately apparent from the form of the energy equations in the previous section that the source tilt function should be continuous across the cell boundaries, as otherwise energy will flow between the cells at a rate which depends only on the cell size rather than on the properties of the material. This is the behaviour exhibited by piecewise constant treatments of the emissivity often referred to as teleportation error [19]; here we are excluding the effect which can occur in optically thin cells, due to the possibility of a large physical separation between where a photon is absorbed and the sampled re-emission location, which is not addressed by the source tilt schemes, and can be thought of as a temporal discretisation error arising from the coarse spatial mesh.

SIMC schemes are more prone to teleportation error due to the larger coefficient in these jump terms, whereas for IMC schemes this excess energy flux is scaled down by a factor $\sqrt{f_i}$. Provided the Fleck parameter can be chosen to scale as ϵ^2, it can be shown that the IMC method with a piecewise constant representation of temperature has a valid asymptotic diffusion limit [9]; the energy transport is no longer localised to nearest neighbour cells as $\sqrt{f}\tau$ is now an 0(1) quantity.

This behaviour is a consequence of the extended lifetime of the Monte Carlo particles, which ensures that the contribution to the particle field from particles created by the residual thermal emission source term (which scales as f) during the time-step is small enough relative to the contribution from the pseudo-scattering term (which scales as $1 - f$) to the thermal emission from the material that any excess flow associated with the boundary layer

caused by jumps in this function is of order ϵ relative to the energy flow due to the ambient radiation field.

We have not discussed the time discretisation of the deterministic scheme, but similar procedures to the SIMC and IMC time discretisations can be employed in order to treat the time evolution of these equations. Typically, we follow the approach of the IMC method in order to derive a set of linearised discrete transport equations for the radiation field [20]. This semi-implicit approach leads to similar modifications to the terms in the total energy equation, although we use smaller time-steps than are typically used with the IMC method as we attempt to accurately capture the details of the time-dependent evolution i.e. we do not rely on time-stepping to help reduce the discretisation errors and instead focus on achieving accurate results in the limit of small time-steps where the form of the equations is unchanged.

6. The Reconstruction Process

The source tilt problem can be stated as follows. Given a set of cell centred temperatures, T_i, reconstruct nodal and cell average values of Φ such that the total energy equation corresponds to an accurate discretisation of the associated diffusion problem while maintaining a level of consistency between the cell average Φ value, $\overline{\Phi}_i$, and the value derived from the cell averaged temperatures $\Phi_i = acT_i^4/(4\pi)$.

We note that it is also possible to derive sub-cell schemes where the emissions are localised to a smaller sub-domain than the entire cell. These schemes can also be analysed using the current methodology by treating these sub-domains as additional cells in the problem, but combining the results in these sub-cells in order to derive the corresponding cell centred energy equation.

Several approaches can be followed in order to derive an improved spatial variation for the emissivity. An alternative to using the cell temperatures to derive the emission profiles is to include extra tallies when solving the transport problem and determine the spatial gradients from these tallies [21]. This approach can lead to the introduction of significant additional noise into the simulations, especially in 2 and 3 dimensions for problems where the number of particles passing through the cells is insufficient to generate meaningful statistics for these gradient tallies.

Consequently, we focus on schemes based solely on the cell centred temperature information. Rather than undertake an exhaustive study of different

source tilt schemes, this paper focuses on results from the asymptotic analysis for the slope based tilt scheme described by Fleck and Canfield [22]. Future work will focus on the accuracy of various source tilt schemes based on the analysis contained in this paper.

6.1. Gradient based approach

Fleck and Canfield proposed a source tilt scheme based on reconstructing the cell averaged gradients of Φ, $\overline{\nabla\Phi}_i$, assuming $\overline{\Phi}_i = \Phi_i$. These slopes are used to bias the distribution of the emission locations, but (as with the piecewise constant formulation) the *magnitude* of the emission is determined directly from the cell averaged Φ values, which means that the reconstructed Φ function changes discontinuously from cell to cell. In slab geometry we have

$$\Phi_{i,L} = \Phi_i - \frac{1}{2}\Delta\Phi_i, \;\; \Phi_{i,R} = \Phi_i + \frac{1}{2}\Delta\Phi_i \tag{54}$$

where $\Delta\Phi_i = \langle\frac{\partial\Phi}{\partial x}\rangle_i \Delta x_i$ is the difference between the right and left Φ values in cell i.

One of the authors (McClarren) has previously investigated the behaviour of these schemes in slab geometry, for a P_n angular discretisation [23]; to the authors' knowledge this is the first time that a source tilt scheme has been applied in the context of a deterministic approach for solving thermal radiation transport problems.

Using this slope based formulation of the tilt, we can derive results for both continuous and discrete forms of the transport equation in terms of the slopes and the cell average values of Φ. The equations are:

$$\begin{aligned}
&\frac{1}{4\pi}\left[(\rho C_V)_i\frac{\partial T_i}{\partial t} + \frac{\partial U_i}{\partial t}\right]\Delta x_i = \\
&\quad +\eta(c_i \to c_{i+1})(1-c_i)\delta\Phi_{i+\frac{1}{2}} - \eta(c_i \to c_{i-1})(1-c_i)\delta\Phi_{i-\frac{1}{2}} \\
&\quad +(1-\theta(c_i \to c_{i+1}))\frac{\Delta\Phi_{i+1}}{3\tau_{i+1}} + \theta(c_i \to c_{i+1})\frac{\Delta\Phi_i}{3\tau_i} \\
&\quad -(1-\theta(c_i \to c_{i-1}))\frac{\Delta\Phi_{i-1}}{3\tau_{i-1}} - \theta(c_i \to c_{i-1})\frac{\Delta\Phi_i}{3\tau_i}
\end{aligned} \tag{55}$$

for the continuous transport equation and:

$$\frac{1}{4\pi}\left[(\rho C_{\mathrm{V}})_i\frac{\partial T_i}{\partial t}+\frac{\partial U_i^*}{\partial t}\right]\Delta x_i = +\frac{1}{4}\delta\Phi^*_{i+\frac{1}{2}}-\frac{1}{4}\delta\Phi^*_{i-\frac{1}{2}} + \frac{1}{6\tau_{i+1}}\left(\Delta\Phi_{i+1}-2\delta\Phi_{i+\frac{3}{2}}\right)+\frac{1}{6\tau_i}\left(\Delta\Phi_i-2\delta\Phi_{i-\frac{1}{2}}\right) - \frac{1}{6\tau_{i-1}}\left(\Delta\Phi_{i-1}-2\delta\Phi_{i-\frac{3}{2}}\right)-\frac{1}{6\tau_i}\left(\Delta\Phi_i-2\delta\Phi_{i+\frac{1}{2}}\right) \quad (56)$$

for the linear discontinuous form of the equations. Here $\delta\Phi_{i+\frac{1}{2}} = (\Phi_{i+1} - \Phi_i) - \frac{1}{2}(\Delta\Phi_i + \Delta\Phi_{i+1})$ is the jump in Φ across the interface between cells i and $i+1$ and $\delta\Phi^*_{i+\frac{1}{2}} = (\Phi^*_{i+1,L} - \Phi^*_{i,R}) \rightarrow \delta\Phi_{i+\frac{1}{2}}$ in the absence of scattering.

6.1.1. Slope reconstruction

One of the simplest schemes for constructing the slopes makes use of a central difference approximation for the gradient derived from the cell average values of Φ its direct neighbours,

$$\Delta\Phi_i \;=\; \Delta x_i(\Phi_{i+1}-\Phi_{i-1})/(\overline{x}_{i+1}-\overline{x}_{i-1}) \quad (57)$$

This provides a second order accurate approximation of the derivative on uniform meshes, which is equivalent to performing a least squares fit for the gradient. For the cells on the problem boundaries we use first order gradients calculated in the interior.

This could be supplemented by first order gradients calculated at the left and right boundaries of the cell. Using this information, a strategy could be devised for combining these various different approximations for the derivatives in order to compute a slope within the element which satisfies local monotonicity conditions. In this paper we do not explore the issue of employing slope limiters to improve the behaviour in the vicinity of local extrema any further. Instead, we restrict the magnitude of the slope so that the reconstruction remains positive throughout the cell, $|\Delta\Phi_i| \leq 2\Phi_i$. This is the simplest source tilt scheme and it will be shown to significantly improve the spatial convergence of the transport calculations.

However, it still leaves discontinuities in the reconstruction of the Φ function at cell boundaries. The magnitude of these jump terms is controlled by both the cell size and the smoothness of the function, but they are in general much larger than the gradient terms in significantly opaque cells as

they do not involve the reciprocal of the cell optical depth. Consequently, these schemes require much finer meshes than the equivalent finite difference diffusion schemes due to the presence of these additional error terms, which will the dominate the spatial convergence behaviour.

6.2. Continuous variants

A more accurate alternative to the slope based tilt scheme described above can be obtained by simply replacing the discontinuous nodal values by a continuous set of values in the problem interior, obtained by a simple averaging scheme,

$$\Phi_{i,R} = \Phi_{i+1,L} = \frac{1}{2}\left(\Phi_i + \Phi_{i+1}\right) + \frac{1}{4}\left(\Delta\Phi_i - \Delta\Phi_{i+1}\right) = \Phi_{i+1/2} \tag{58}$$

The jumps persist at the problem boundaries, as we apply a separate treatment of the incident and exiting radiation field i.e. the boundary conditions are weakly enforced in order to avoid seeding oscillations in the problem interior.

However, this simplest of continuous tilt schemes suffers from a saw-tooth instability mode on a uniform mesh (in the absence of scattering), as the corresponding discrete equilibrium diffusion equation for cell i depends only on Φ_{i-2}, Φ_i and Φ_{i+2}. The energy equations for even and odd cells are decoupled, leading to two independent temperature profiles that are coupled only at the problem boundaries. This manifests itself as a lack of smoothness in the cell-wise profile, although the separate profiles constructed from the odd and even points both converge point-wise towards the correct solution as the mesh is refined.

This difficulty can be overcome by subdividing each cell i into two parts (at $x = \overline{x}_i$) and changing the interpolation so that the reconstructed profile passes through the element average value at this point:

$$\Phi(x) = \begin{cases} \Phi_{i-1/2}\frac{(\overline{x}_i - x)}{(\overline{x}_i - x_{i-1/2})} + \Phi_i\frac{(x - x_{i-1/2})}{(\overline{x}_i - x_{i-1/2})} & x < \overline{x}_i \\ \Phi_i\frac{(x_{i+1/2} - x)}{(x_{i+1/2} - \overline{x}_i)} + \Phi_{i+1/2}\frac{(x - \overline{x}_i)}{(x_{i+1/2} - \overline{x}_i)} & x > \overline{x}_i \end{cases} \tag{59}$$

We locate the cut at the midpoint $\overline{x}_i = (x_{i-1/2} + x_{i+1/2})/2$ and refer to this scheme as the sub-cell continuous variant. Neither of these schemes matches the cell average value i.e. $\overline{\Phi}_i \neq \Phi_i$ for cell i. It would be possible to vary the location of the inflection point so as to match the cell average value, provided this average lies in-between the two nodal values[24]; unfortunately this would be difficult to generalise to multi-dimensions.

7. Results

In order to generate numerical results for comparison with the asymptotic expressions derived in this paper we solve the following transport problem using a linear discontinuous discretisation of the S_n equations:

$$\begin{aligned} \frac{1}{c}\frac{\partial \Psi(\mu,x,t)}{\partial t} &+ \mu\frac{\partial}{\partial x}\Psi + \sigma_i\Psi \\ &= \sigma_i\Phi(x,t) = \sigma_i\left(\Phi_{i,L}(t)b_1(x) + \Phi_{i,R}(t)b_2(x)\right), \end{aligned} \tag{60}$$

where the transport mesh may be chosen to be considerably finer than the temperature mesh. This is coupled to the set of cell material energy equations:

$$(\rho C_V)_i\frac{\partial T_i}{\partial t}\Delta x_i = 2\pi\int_{x_{i-\frac{1}{2}}}^{x_{i+\frac{1}{2}}}\int_{-1}^{1}\sigma_i(\Psi(\mu,x,t)-\Phi(x,t))d\mu dx. \tag{61}$$

Fine mesh transport solutions are used as an alternative to generating a converged Monte Carlo solution to validate the continuum transport results.

For discontinuous reconstructions with large discontinuities, converging the transport solution may require meshes fine enough to resolve the boundary layers associated with the jumps at the interface. However, the temperature mesh must remain sufficiently coarse that the local coupling approximation remains valid, otherwise the predictions from the expressions in this paper will not match the transport results.

We note that the results from the asymptotic analysis are computed assuming that the cells are in thermal equilibrium i.e. we compute the total cell energy change and then use this to compute an updated equilibrium material temperature in each cell, rather than evaluating the radiation energy contribution to the time derivative consistently with the source tilt. This slight inconsistency with the detailed analysis does not adversely affect the accuracy of the predictions, as the material energy is always significantly larger than the radiation energy density for the Marshak wave problem.

7.1. Piecewise constant results

We begin by considering the effects of resolution on the results for a piecewise constant treatment of the emissivity. All the results presented in this paper are generated for the temperature dependent Marshak wave problem considered by McClarren and Lowrie [25], which provides a stringent test of the diffusion limit behaviour.

This problem is driven by a constant 1 keV temperature source on the left boundary. The material properties are $\sigma = 300\,T^{-3}$ cm^{-1} with T measured in keV; the heat capacity is $C_V = 0.3 \times 10^{16}$ erg/cm^3/keV. The initial condition is $T = 1.0 \times 10^{-6}$ keV with the radiation in equilibrium with the material. In order to include coarse meshes the length of the slab is doubled from 0.6 cm to 1.2 cm and although the original problem was defined to have a reflecting boundary on the right, we perform these calculations by setting $\Phi_R = 0$ and allowing radiation to escape from both ends of the domain.

7.1.1. Pure absorber ($f = 1$)

We begin by plotting the results for the no-scattering case, i.e., where we are not relying on the scattering process to improve the accuracy of the piecewise constant treatment of material temperature. Figures 2 and 3 show the results from time-converged solutions of both the asymptotic limit equations (46), (47) and also from S_n calculations, for a variety of mesh resolutions at 10 shakes (1 shake = 10 ns) after the drive is imposed. High resolution simulations indicate that the wave should have propagated distance of 0.15 cm, so even with the finer meshes there is significant excess numerical diffusion.

There is excellent agreement between the asymptotic limit of the lumped equations (47) and the solution of the lumped S_n equations coupled to the material energy equations for optically thick meshes; note that the asymptotic limit reduces to (51) for a piecewise constant variation. Furthermore, refining the transport mesh (for a fixed temperature grid) has little effect on these results except on the finest meshes, as predicted from the asymptotic analysis of the continuum transport problem (see Figure 3).

The agreement between the asymptotic limit of the un-lumped equations and the solution of the un-lumped S_n equations is also excellent on the coarse meshes, however it degrades at finer mesh resolutions due to the presence of the extra $O(\epsilon)$ terms in (46). As observed previously, simply doubling the resolution of the transport mesh in the S_n equations (but keeping the temperature mesh unchanged) eliminates these extra terms and yields solutions which closely match the lumped asymptotic limit.

At finer resolutions the transport solutions begin to deviate from the asymptotic behaviour as shown in figure 4. Both lumped and un-lumped solutions converge to the same continuum transport limit, with the lumped solutions exhibiting significantly greater accuracy for the same transport mesh resolution. This behaviour is in sharp contrast to the convergence of the equations for a linear source term (or as we will see in the next section for

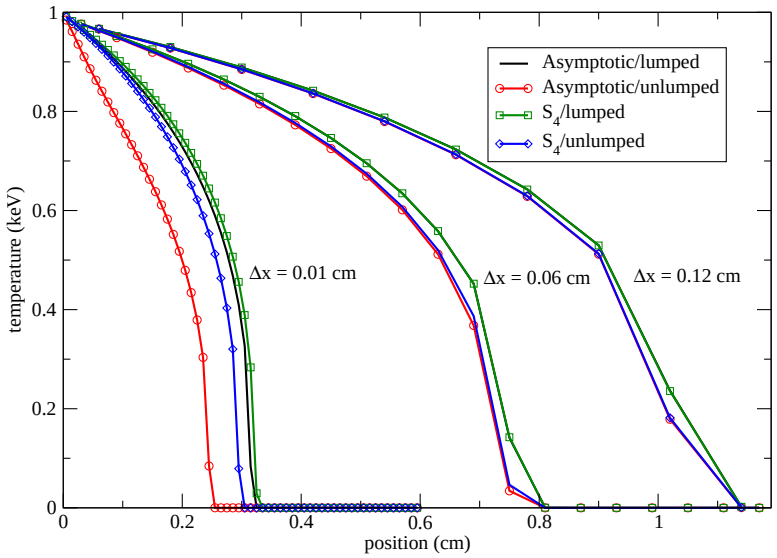

Figure 2: Plot of temperature at 10 shakes using a piecewise constant representation of temperature ($f = 1$), for mesh resolutions of 0.12, 0.06, and 0.01 cm. Here the asymptotic limit predictions are compared with S_4 transport results. Note that even the fine mesh simulations have significantly overestimated the wave speed, as the wave should only have propagated a distance 0.15 cm.

problems with significant scattering), where mass lumping degrades the convergence rate.

7.1.2. Scattering problem with $f = 0.1$

We now consider the behaviour of the transport problem for a lower value of the Fleck parameter, in order to understand the behaviour of the pseudo-scattering term on the discretised transport equation. The mesh must be sufficiently coarse that the constraints on the asymptotic analysis remain valid, so we are limited to considering only modest scattering ratios. The spatial convergence of the transport solutions is compared in figure 5 for lumped solutions and figure 6 for unlumped solutions (the temperature mesh is unchanged), to illustrate how the results transition from the discretised asymptotic limit to the continuum limit.

The asymptotic limit of the continuum transport equations shows a reduction in the amount of excess numerical diffusion (but by less than the factor $3 \approx 1/\sqrt{f}$ inferred from the scaling of the jump terms). This prediction is closely matched by the solution of the discrete equations as the

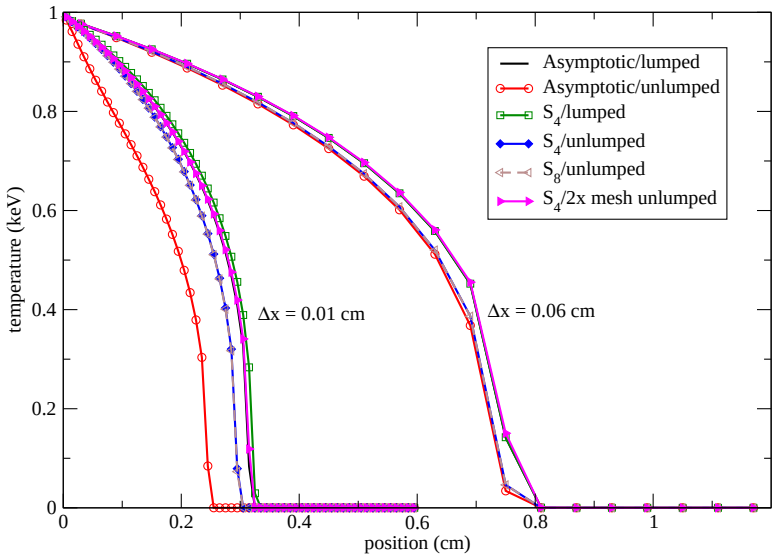

Figure 3: Plot of temperature at 10 shakes using a piecewise constant representation of temperature ($f = 1$), for mesh resolutions of 0.06, and 0.01 cm. Here the asymptotic limit predictions and S_4 transport results from Figure 2 are compared with S_8 unlumped solutions and S_4 unlumped solutions with a refined radiation grid. Here we see no discernible difference between the S_4 and S_8 unlumped solutions; the S_4 unlumped 2x mesh solutions and the asymptotic lumped solutions also agree, as predicted by our analysis.

transport mesh is refined. However, for the coarser transport meshes, the solution is much closer to the results for zero scattering, illustrating that the linear discontinuous discretisation does not accurately represent the effect of scattering on coarse meshes.

This lack of accuracy is a consequence of the inability of the spatial discretisation of the transport problem to model the localised boundary layers which develop in the vicinity of the discontinuities in the source term [9], for non-zero scattering ratios. Furthermore, this illustrates that the introduction of scattering into the discrete transport equation does not have the same dramatic effect, in terms of reducing the excess energy flow, as for the continuum transport equation. This explains why the relative success of the use of a lower order representation of the material temperature, for Monte Carlo thermal radiation transport, does not carry over to deterministic methods based on similar semi-implicit linearisation techniques applied to the time evolution.

Indeed, this helps to explain the significant differences in the histories of

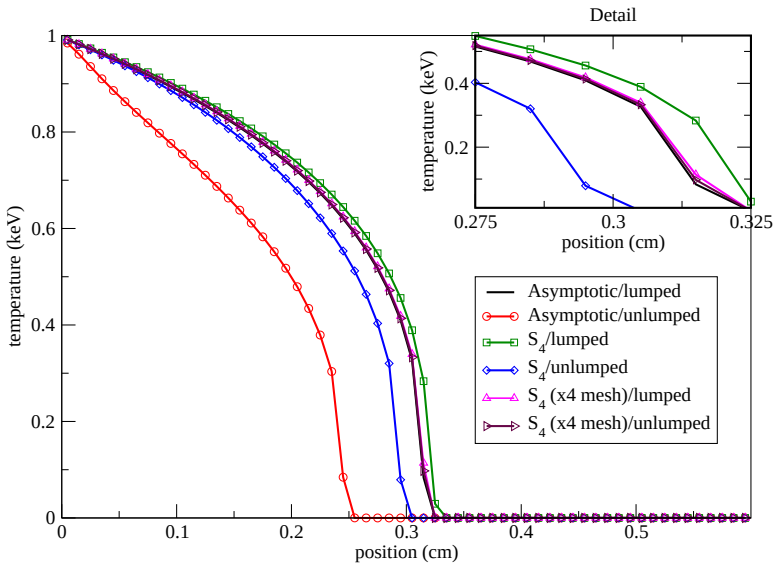

Figure 4: Plot of temperature at 10 shakes using a piecewise constant representation of temperature ($f = 1$), for a mesh resolution of 0.01 cm. Here the asymptotic limit predictions are compared with S_n transport results at increased spatial resolutions (for the same fixed temperature grid). Inset is a blow-up of the region close to the calculated wavefront which illustrates that (as expected) the transport results are converging to a result close to the asymptotic lumped solution i.e. the limit corresponding to the continuum transport problem.

the developments of the two approaches, with the importance of a consistent linear treatment of the material temperature (underwritten by an analysis of the behaviour in the asymptotic diffusion limit) being fundamental to the success of deterministic methods applied to solve thermal radiation transport problems on coarse (optically thick) meshes.

7.2. Slope reconstruction

We repeat the Marshak wave problem with different mesh resolutions to illustrate the spatial convergence of the slope reconstruction approaches. We compare the asymptotic limit predictions and S_n transport solutions in figure 7. As expected the results are a significant improvement on the convergence of the piecewise constant results, but there is still a significant variation in the results for resolutions where the mesh cells remain optically thick. We also note the similarities between these results and the analysis of the slope limiters applied to LD methods with a consistent linear temperature variation

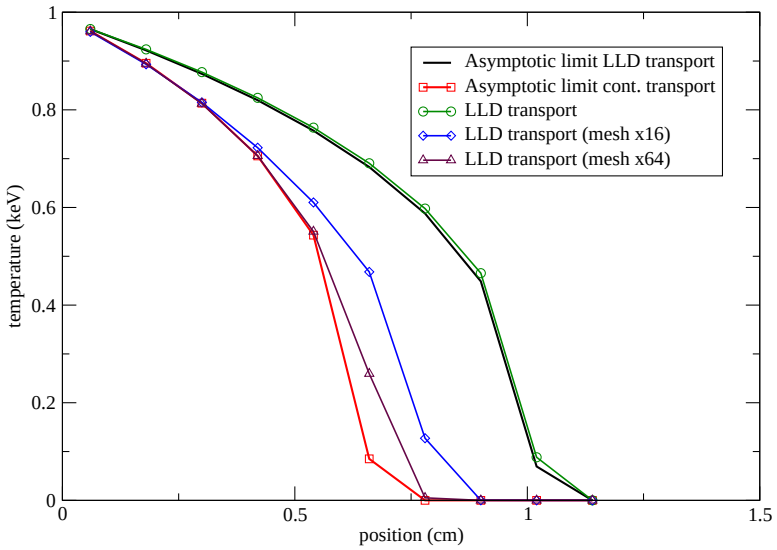

Figure 5: Plot of temperature at 10 shakes using a piecewise constant representation of temperature ($f = 0.1$), for a temperature mesh resolution of 0.12 cm. Here the asymptotic limit predictions are compared with lumped S_n transport results at increased spatial resolutions (for the same fixed temperature grid) illustrating the transition from the discrete to the continuum asymptotic limits for lumped solutions. Note "LLD" refers to a lumped, linear-discontinuous discretization.

by McClarren and Lowrie [25]. In those previous results, the use of a slope limiter that does not preserve continuity of the material temperature led to the solution moving too fast on coarse grids.

7.3. Continuous variant

Our final results illustrate the behaviour of the continuous variant of the slope scheme. The benefits obtained from employing the sub-cell scheme are explored, this scheme generating smoother temperature profiles due to the superior properties of the corresponding discrete diffusion equation. We note however that the temperature profile has advanced a similar distance in both cases. The lumped and un-lumped asymptotic limits are identical except at the boundaries, but this again leads to the un-lumped solutions lagging behind the lumped/continuous transport limit.

The behaviour of the asymptotic limits is similar to the results for slope scheme discussed in the previous section, so rather than presenting these results we focus on comparing the continuous tilt and its sub-cell variant at two different mesh resolutions. We restrict ourselves to presenting the

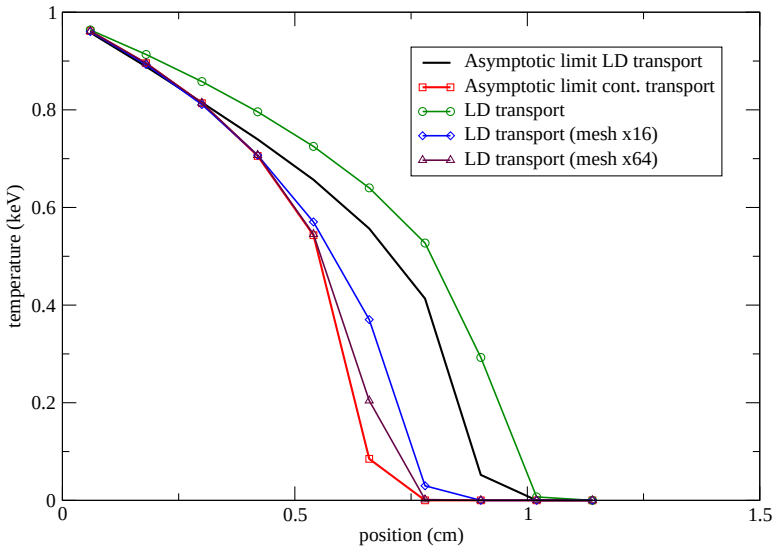

Figure 6: Plot of temperature at 10 shakes using a piecewise constant representation of temperature ($f = 0.1$), for a temperature mesh resolution of 0.12 cm. The unlumped linear-discontinuous (LD) transport solutions converge much faster than the equivalent lumped results as we refine the transport mesh for this scattering dominated problem. The discrete asymptotic limit for the unlumped discretisation is also significantly less accurate than for the lumped discretisation at the same mesh resolution.

lumped S_4 transport results in figure 8, where the discrete transport solution is already mesh converged for a given linear variation of Φ; the systematic behaviour would be similar for both the un-lumped transport scheme and also for the corresponding asymptotic limits.

From these results we see that even these simplest of continuous tilt schemes are notable in having completely removed the spurious numerical diffusion observed in the previous results, the Marshak wave structure being remarkably well resolved especially for the sub-cell scheme. This is consistent with the predictions of our asymptotic analysis, which indicates the necessary requirements for the tilt scheme in order to produce accurate results for diffuse problems; the continuous tilt variants are designed to meet these requirements.

8. Conclusions

In this paper we have presented a unified analysis of both continuum e.g. Monte Carlo and linear discontinuous spatial treatments applied to the

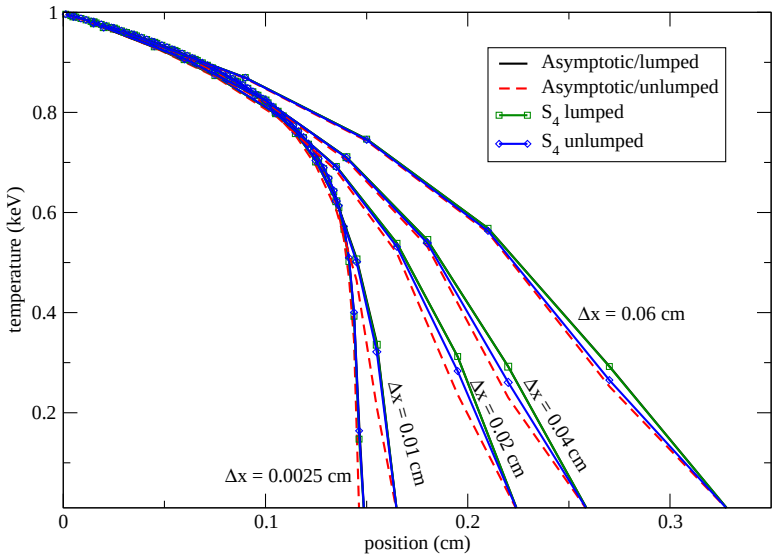

Figure 7: Plot of temperature at 10 shakes using the slope based reconstruction scheme for mesh resolutions of 0.06, 0.04, 0.02, 0.01 and 0.0025 cm. Here the asymptotic limit predictions are compared with S_n transport results for a range of resolutions. On coarse meshes the asymptotic limits correctly predict the differences between the two sets of transport solutions, whereas on fine meshes the transport solutions coincide with the more accurate lumped asymptotic limit.

thermal radiation transport equation, for a linear treatment of the emissivity coupled to a cell centred energy equation. Both purely absorbing and scattering dominated media are considered, the scattering assumed to be a consequence of the temporal discretisation schemes used to ensure stability for time-steps larger than the relaxation time of the medium; Thomson scattering is generally insignificant for laser fusion targets due to their small size.

The results of this analysis are supported by numerical predictions for both no scattering and scattering dominated problems, illustrating the effect of scattering on the asymptotic behaviour of the transport problem. These results illustrate the poor convergence of the piecewise constant treatment of the emissivity and confirm that this is diminished by the presence of the scattering term in the continuum transport equation, an effect which is not reproduced by the linear discontinuous spatial discretisation.

The introduction of a linear variation into the emissivity significantly improves the accuracy of the results and is to be preferred over the abuse of

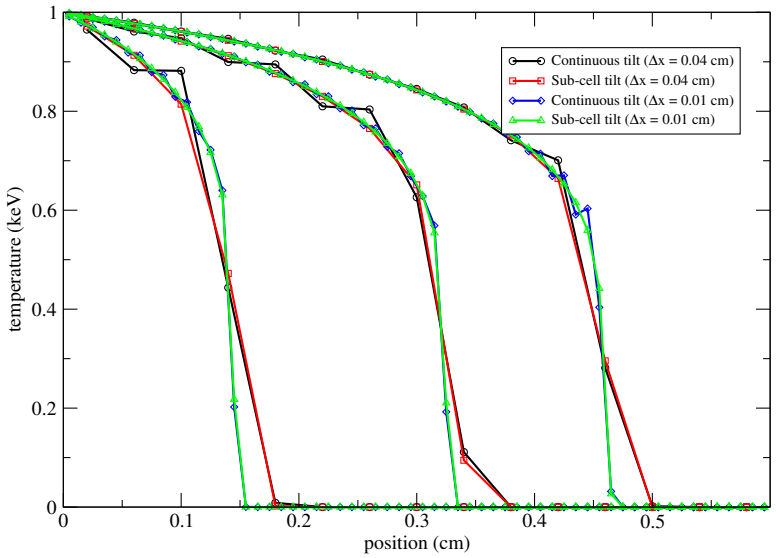

Figure 8: Plots of temperature at 10, 50, and 100 shakes using the continuous tilt scheme and its sub-cell variant for mesh resolutions of 0.04 and 0.01 cm. Here the results from S_4 transport simulations are presented at the two different resolutions. The continuous tilt schemes accurately predict the distance of the wave propagation even for the coarse mesh, the profile being as well resolved as could be anticipated for such a coarse mesh.

the temporal stabilisation mechanism (by using artificially large time-steps) in order to reduce teleportation errors. However, despite the improvements to the convergence, this does not provide a tractable solution for under-resolved optically thick regions such as the gold wall in a 3D simulation of a laser hohlraum. Enforcing continuity in the tilt scheme potentially overcomes these limitations, permitting the use of coarser meshes which are sufficient to represent the temperature variation but without the need to resolve the radiation mean free path.

The results presented in this paper are focused on the discontinuous reconstructions most commonly used by IMC codes in slab geometry. Significant scope remains for a more detailed study of improvements to tilt schemes based on the results of this analysis, focused on retaining continuity between cells in order to improve the spatial convergence behaviour for optically thick problems. Early results indicate that this approach is effective at improving the spatial convergence behaviour not only in slab geometry but also for multi-dimensional problems.

9. Acknowledgements

Thanks to Professor Mike Williams (Visiting Professor at Imperial College) for directing one of the authors (Smedley-Stevenson) to Ted Auerbach's work [26] and providing the relevant extract. This prompted a more thorough investigation of the analytic solutions of these two half-spaces scattering problems and led to the derivation of new results for linearly varying isotropic sources [13]. The results relevant to this paper are summarised in Appendix A.

Appendix A. Further details on the coupling coefficients

In addition to the purely absorbing limits, the η coefficient has the following closed form expression [26].

$$\eta(c_1 \to c_2)(1-c_1) = \frac{1}{2}(1-c_1)(1-c_2)\left[\frac{\frac{c_2 h_1(c_2)}{\sqrt{1-c_2}} - \frac{c_1 h_1(c_1)}{\sqrt{1-c_1}}}{c_2 - c_1}\right] \tag{A.1}$$

where

$$h_1(c) = \int_{\mu=0}^{1} \mu H(\mu, c) d\mu \tag{A.2}$$

is the first moment of Chandrasekhar's H-function [27] for isotropic scattering in a medium with single scattering albedo c. It is a monotonically increasing function of c which varies from $h_1(0) = \frac{1}{2}$ to $h_1(1) = 2/\sqrt{3}$; Stibbs and Weir [28] contains a set of polynomial fits to this function over the entire range of c values.

For $c_2 \to 0$ and $c_1 \neq c_2$ we have:

$$\begin{aligned} \eta(c_1 \to 0)(1-c_1) &= \eta(0 \to c_1) = \frac{1}{4}(1-\alpha(c_1)) \\ &= \frac{1}{2}\sqrt{1-c_1}\, h_1(c_1) \end{aligned} \tag{A.3}$$

As $c_2 \to c_1$ we have

$$\eta(c_1 \to c_2)(1-c_1) = \frac{1}{2}\sqrt{1-c_1}\left[\left(1 - \frac{c_1}{2}\right) h_1(c_1) + c_1(1-c_1) h_1'(c_1)\right] \tag{A.4}$$

$\eta(c_1 \to c_2)$				$\theta(c_1 \to c_2)$			
c_1/c_2	0.0	0.5	0.9	c_1/c_2	0.0	0.5	0.9
0.0	0.25	0.21	0.13	0.0	0.50	0.43	0.27
0.5	0.43	0.37	0.24	0.5	0.57	0.50	0.31
0.9	1.30	1.20	0.89	0.9	0.73	0.69	0.50

Table A.1: Sample values of the η and θ coefficients for c=0, 0.5 and 0.9

where the term in square brackets in the first expression is a slowly varying function that monotonically increases from $1/2$ for $c_1 = 0$ to $1/\sqrt{3}$ for $c_1 = 1$. These derivatives have been tabulated by Viik [29].

A similar approach can be used to derive an analytic expression the θ coefficient [13]

$$\begin{aligned} \theta(c_1, c_2) &= \frac{1}{2} - \frac{3}{8}\frac{(1-c_1)(1-c_2)}{(c_2-c_1)}\left\{\frac{c_2 h_1(c_2)}{\sqrt{1-c_2}} - \frac{c_1 h_1(c_1)}{\sqrt{1-c_1}}\right\}^2 \\ &= 1 - \theta(c_2, c_1) \end{aligned} \tag{A.5}$$

In table A.1 we have tabulated these coefficients for three different values of the scattering ratio. It is possible to design an efficient procedure for evaluating these functions for arbitary values of c_1 and c_2 [13], although this is not required in order to reproduce the results presented in this paper.

[1] J. Morel, R. M. Roberts, M. J. Shashkov, A local support-operators diffusion discretization scheme for quadrilateral r-z meshes, Journal of Computational Physics 144 (1) (1998) 17 – 51. doi:10.1006/jcph.1998.5981.
URL http://www.sciencedirect.com/science/article/pii/S0021999198959812

[2] J. M. Nordbotten, G. T. Eigestad, Discretization on quadrilateral grids with improved monotonicity properties, Journal of Computational Physics 203 (2) (2005) 744 – 760. doi:10.1016/j.jcp.2004.10.002.
URL http://www.sciencedirect.com/science/article/pii/S0021999104004036

[3] M. L. Adams, Subcell balance methods for radiative transfer on arbitrary grids, Transport Theory and Statistical Physics 26 (4-5) (1997) 385–431. doi:10.1080/00411459708017924.
URL http://www.tandfonline.com/doi/abs/10.1080/00411459708017924

[4] J. D. Edwards, J. E. Morel, R. B. Lowrie, Second-order discretization in space and time for radiation hydrodynamics, in: International Conference on Mathematics and Computational Methods Applied to Nuclear Science and Engineering (M&C 2013), American Nuclear Society, LaGrange Park, IL, 2013, on CD-ROM.

[5] G. C. Pomraning, The Equations of Radiation Hydrodynamics, Dover Publications, Mineola, New York, 2005.

[6] E. Larsen, G. Pomraning, V. Badham, Asymptotic analysis of radiative transfer problems, Journal of Quantitative Spectroscopy and Radiative Transfer 29 (4) (1983) 285 – 310. doi:10.1016/0022-4073(83)90048-1.
URL http://www.sciencedirect.com/science/article/pii/0022407383900481

[7] J. E. Morel, B. T. Adams, T. Noh, J. M. McGhee, T. M. Evans, T. J. Urbatsch, Spatial discretizations for self-adjoint forms of the radiative transfer equations, Journal of Computational Physics 214 (1) (2006) 12 – 40. doi:10.1016/j.jcp.2005.09.017.
URL http://www.sciencedirect.com/science/article/B6WHY-4HHP5D4-1/2/1b3108a5cb

[8] R. P. Smedley-Stevenson, A linear SIMC scheme suitable for extension to multidimensions, in: International Conference on Mathematics, Computational Methods & Reactor Physics (M&C 2009), American Nuclear Society, LaGrange Park, IL, 2009, on CD-ROM.

[9] J. D. Densmore, Asymptotic analysis of the spatial discretization of radiation absorption and re-emission in Implicit Monte Carlo, Journal of Computational Physics 230 (4) (2011) 1116 – 1133. doi:10.1016/j.jcp.2010.10.030.
URL http://www.sciencedirect.com/science/article/B6WHY-51C4RXT-1/2/042b177dab

[10] G. Collins, The Fundamentals of Stellar Astrophysics, W.H. Freeman, 1989.
URL http://books.google.co.uk/books?id=QFtnQgAACAAJ

[11] E. D. Brooks III, Symbolic implicit Monte Carlo, Journal of Computational Physics 83 (2) (1989) 433 – 446. doi:10.1016/0021-9991(89)90129-0.
URL http://www.sciencedirect.com/science/article/pii/0021999189901290

[12] J.-F. Clouët, G. Samba, Asymptotic diffusion limit of the symbolic Monte-Carlo method for the transport equation, Journal of Computational Physics 195 (1) (2004) 293 – 319. doi:10.1016/j.jcp.2003.10.008.
URL http://www.sciencedirect.com/science/article/pii/S0021999103005333

[13] R. P. Smedley-Stevenson, A new analytic solution of the one-speed neutron transport equation for adjacent half-spaces with isotropic scattering, Annals of Nuclear Energy 46 (0) (2012) 218 – 231. doi:10.1016/j.anucene.2012.03.034.
URL http://www.sciencedirect.com/science/article/pii/S0306454912001132

[14] J. A. Fleck, Jr., J. D. Cummings, An Implicit Monte Carlo scheme for calculating time and frequency dependent nonlinear radiation transport, Journal of Computational Physics 8 (1971) 313–342.

[15] E. W. Larsen, J. Morel, W. F. Miller Jr., Asymptotic solutions of numerical transport problems in optically thick, diffusive regimes, Journal of Computational Physics 69 (2) (1987) 283 – 324. doi:10.1016/0021-9991(87)90170-7.
URL http://www.sciencedirect.com/science/article/pii/0021999187901707

[16] R. G. McClarren, J. P. Holloway, T. A. Brunner, T. A. Mehlhorn, A quasilinear implicit riemann solver for the time-dependent P_n equations, Nuclear Science and Engineering 155 (2) (2007) 290–299.

[17] R. McClarren, J. P. Holloway, T. Brunner, T. Mehlhorn, Implicit riemann solvers for the P_n equations, Lecture Notes in Computational Science and Engineering 48 (2006) 457.

[18] A. Buchan, C. Pain, M. Eaton, R. Smedley-Stevenson, A. Goddard, Linear and quadratic octahedral wavelets on the sphere for angular discretisations of the boltzmann transport equation, Annals of Nuclear Energy 32 (11) (2005) 1224 – 1273. doi:10.1016/j.anucene.2005.01.005.
URL http://www.sciencedirect.com/science/article/pii/S0306454905000356

[19] M. S. McKinley, E. D. Brooks III, A. Szöke, Comparison of implicit and symbolic implicit Monte Carlo line transport with frequency weight vector extension, Journal of Computational Physics 189 (1) (2003) 330 – 349. doi:10.1016/S0021-9991(03)00213-4.
URL http://www.sciencedirect.com/science/article/pii/S0021999103002134

[20] J. Morel, T. A. Wareing, K. Smith, A linear-discontinuous spatial differencing scheme for Sn radiative transfer calculations, Journal of Computational Physics 128 (2) (1996) 445 – 462. doi:10.1006/jcph.1996.0223.
URL http://www.sciencedirect.com/science/article/pii/S0021999196902235

[21] J. R. Cheatham, Truncation analysis and numerical method improvements for the thermal radiative transfer equations, Ph.D. thesis, University of Michigan (2010).
URL http://hdl.handle.net/2027.42/75852

[22] J. A. Fleck, Jr., E. H. Canfield, A random walk procedure for improving the computational efficiency of the Implicit Monte Carlo method for nonlinear radiation transport, Journal of Computational Physics 54 (1984) 508–523.

[23] R. G. McClarren, R. B. Lowrie, Effects of the temperature discretization on numerical methods for thermal radiation transport, in: International Conference on Mathematics, Computational Methods & Reactor Physics (M&C 2009), American Nuclear Society, LaGrange Park, IL, 2009, on CD-ROM.

[24] R. T. Wollaeger, T. J. Urbatsch, A. B. Wollaber, J. D. Densmore, An analysis of source tilting and sub-cell opacity sampling for IMC, Tech.

Rep. LA-UR-12-23258, LANL, LANL Student Symposium August 8 (2012).

[25] R. G. McClarren, R. B. Lowrie, The effects of slope limiting on asymptotic-preserving numerical methods for hyperbolic conservation laws, Journal of Computational Physics 227 (23) (2008) 9711 – 9726. doi:10.1016/j.jcp.2008.07.012.
URL http://www.sciencedirect.com/science/article/B6WHY-4T542KX-1/2/b2b25e0b0e

[26] T. Auerbach, Some applications of Chandrasekhar's method to reactor theory, Tech. Rep. BNL 676 (T-255), Brookhaven National Laboratory (1961).

[27] S. Chandrasekhar, Radiative Transfer, Dover, New York, 1960.

[28] D. W. N. Stibbs, R. E. Weir, On the H-functions for isotropic scattering, Monthly Notices of the Royal Astronomical Society 119 (5) (1959) 512–525.

[29] T. Viik, Derivatives of the H-function, Astrophysics and Space Science 204 (1993) 213 – 231.